Development and Testing of a Pre-Prototype Ramgen Engine Budget Period 3 Final Report

March 31, 2002 to October 31, 2003

Principle Author: Ramgen Power Systems

Report Issued July 2003

DOE Award Number: DE-FC26-00NT40915

Document Number 0800-00075

Submitted by:

Ramgen Power Systems, Inc.
11808 Northup Way, Suite W190
Bellevue, WA 98005
(425) 828-4919

Disclaimer

This report was prepared as an account of work sponsored by an agency of the United States Government. Neither the United States Government nor any agency thereof, nor any of their employees, makes any warranty, express or implied, or assumes any legal liability or responsibility for the accuracy, completeness, or usefulness of any information, apparatus, product, or process disclosed, or represents that its use would not infringe privately owned rights. Reference herein to any specific commercial product, process, or service by trade name, trademark, manufacturer, or otherwise does not necessarily constitute or imply its endorsement, recommendation, or favoring by the United States Government or any agency thereof. The views and opinions of authors expressed herein do not necessarily state or reflect those of the United States Government or any agency thereof.

Abstract

The research and development effort of a new kind of compressor and engine is presented. The superior performance of these two products arises from the superior performance of rotating supersonic shock-wave compression.

Several tasks were performed in compliance with the DOE award objectives. A High Risk Technology review was conducted and evaluated by a team of 20 senior engineers and scientists representing various branches of the federal government. The conceptual design of a compression test rig, test rotors, and test cell adaptor was completed. The work conducted lays the foundation for the completed design and testing of the compression test rig, and the design of a supersonic shock-wave compressor matched to a conventional combustor and turbine.

Table of Contents

1   Executive Summary

This report summarizes the results of Ramgen Engine development efforts.

The Ramgen engine represents the unique application of ramjet principles to compression and power generation. The Ramgen Rampressor™ will provide superior compressor performance through rotating super sonic shock compression. The Rampressor can be used to drive a conventional turbine to provide superior engine performance and power production. This effort was funded by Department of Energy cooperative agreement number DE-FC26-00NT40915.

The primary objective of advancing the research and development effort on the Ramgen engine was accomplished in the 7 month long Budget Period 3, by reaching significant technological milestones.

- A fundamental approach change was made as a result of a High Risk Technology review held in Ohio. The consensus was to validate the superior performance of rotating shock wave compression before embarking on the more challenging, expensive and highly integrated Ramgen Engine development.
- A test rig design concept was prepared that will:
    - Allow for the demonstration of Ramgen compression
    - Accommodate the critical instrumentation required to validate performance of a disk spinning at super sonic speeds.
    - Ready fit into a local testing facility
    - Support the quick removal and installation of rotor configuration changes
- The super sonic compression rotor design concepts were prepared to:
    - Enable the checkout of the rig systems independently
    - Validate rotor drag
    - Check the critical tip seal clearance control system
    - Provide forgiving starting characteristics
    - Demonstrate compression performance traceable to industry specifications.

The successful accomplishment of these tasks will culminate in the test rig design and compression data in the next budget period (BP4). The successful demonstration of superior compression performance is a critical step to demonstrating superior engine performance on a Rampressor and conventional combustor/turbine which will be designed in the next budget period.

2   Introduction

2.1   Project Objectives

The objectives of Budget Period 3 were two fold. First a detailed evaluation of the Ramgen High Risk Technology was conducted. Additionally, the data from the previous budget period static combustor and inlet testing as well as the design information were integrated into the design of the Rampressor test rig.

These objectives were translated into specific tasks for the Cooperative Agreement:

> Task 8.0 - Design Review of High Risk Technology
> Task 9.0 - Core Engine Program Rig Design
> Task 10.0 - Rotor Cartridge Design
> Task 11.0 - Test Cell Adaptor Design

2.2   Design Review of High Risk Technology

On April 9th and 10th 2002 Ramgen, under the direction of NETL US DOE, assembled a team of approximately 20 senior engineers and scientists representing various branches of the federal government (NASA, Army, USAF, DOE/NETL) to review and evaluate the Ramgen engine technology at the Ohio Aerospace Institute Cleveland.

The evaluation and summary conclusions of the government reviewers were organized by the use of a federal based Technology Readiness Level ("TRL") approach as applied to four distinct aspects of the Ramgen engine technology, namely:

1) The overall technical concept
2) Engineering and design
3) Manufacturing
4) Integration and test

A copy of the Topical report is attached as Attachment 3-1 – Meeting Report, Ramgen Design Review Workshop; dated April 2002.

2.3   Core Engine Program Rig Design

Ramgen has developed a core engine component rig concept focused on the mechanical definition of systems required for validation testing of the rotating supersonic inlet. The goal of the conceptual design was to define mechanical systems to address aerodynamic requirements for the rig, as well as concept systems required for its mechanical operation. A detailed description of these systems is given in Section 4.1. The concept was provided in layout format. The design was the subject of a Conceptual Design Review (CDR) held at Ramgen on September 5, 2002. The purpose of the review was to evaluate the conceptual mechanical layout from a design and manufacturing standpoint, identifying areas of risk or the need for further conceptual design. A summary of the CDR is given in section 4.1.

2.4　Rotor Cartridge Design

Ramgen has developed a conceptual design of a rotor capable of meeting aerodynamic requirements to evaluate a rotating supersonic compression inlet. Methodologies for preliminary sizing of the rotor based on rotational speed have been developed. Proof of concept studies on boundary layer bleed configurations have been performed. Section 4.2.3 details this work.

2.5　Test Cell Adaptor Design

The test cell adapter design focused on the concept of the Rampressor being assembled as a completely self-contained unit, mounted on a "skid" that would contain the drive motor, lube system, all peripheral systems, valving, controls, and data acquisition systems. The skid would be easily adaptable to any test cell and would be transported via fork lift for quick installation. See Section 4.3 for details of this work.

3 Design Review of High Risk Technology

A copy of the meeting report for the Ramgen Design Review Workshop Topical report is attached as Attachment 3-1 – Meeting Report, Ramgen Design Review Workshop; dated April 2002.

4 Core Engine Program Rig Design

4.1 Test Rig Body Design

4.1.1 Aerodynamic/Heat Transfer Design and Analysis

4.1.1.1 Secondary Air System

The following sections deal with the secondary air systems for the Ramgen rotor. The design has been envisioned to be similar for all rotor speeds, whether it is for the Ramgen turbine or for the Ramgen compressor or Rampressor. The analyses discussed in the following sections have been performed for many different rotor speeds ranging from 105,000 rpm to 20,000 rpm. The studied range of rotor speeds was to support the search for an optimally performing engine cycle for the Ramgen engine. The discussion in the following sections is devoted to engine speeds comprising of 105,000 rpm, 49,037 rpm and 40,507 rpm. The discussion regarding other RPM designs will be discussed in a later report.

4.1.1.1.1 Introduction

The secondary airflow network for the Ramgen engine includes the wheel space buffer air, the disc cooling air, the seal leakage air and the bleed air from the main flow path. This section deals with the first two types of secondary air systems and the related effects on the overall engine design while the effects of the bleed flows is discussed in a later report. Since the main airflow path gas ingestion into the wheel space cavity results in excessive disc temperatures, the assignment of wheel space cooling/buffer flows is important in minimizing the effects of such ingestion.

A rotating disc in a rotor-stator cavity creates a radial outflow of fluid within the boundary layer. If no fluid is added to the disc cavity, air from the main flow path ingests inward along the stator into the wheel space cavity and flows radially outward to satisfy the mass flow continuity requirements. Since, such ingestion is not suitable for meeting disk design requirements from a temperature standpoint, the disk and wheel spaces are typically buffered with cooling air. Since any buffer air supplied to the disk cavity is a performance penalty for the engine, judicious use of the cooling air is necessary for meeting the design objectives of the engine. In order to minimize the secondary air being used in the engine, flow discouragers and rim seals are often used in the design of the wheel space cavities.

As mentioned earlier, a rotating disk produces a radial outward flow and this phenomenon is referred to as radial pumping. This radial pumping is dependent on the Reynolds number which determines whether the boundary layer flow is laminar or turbulent. The Reynolds number is defined as

$$\text{Re}_r = \frac{\rho \omega r^2}{\nu}$$

The von Karman solution for pumping rate of a disk rotating in an infinite environment for one face, with turbulent boundary layer, is provided by

$$\dot{m} = C_1 \mu r_o \mathrm{Re}_{ro}^{0.8}$$

When stator walls are included, the flow in the wheel space cavities is modified, and a new parameter represented by G (= s/r_o), called dimensionless gap ratio, is needed to capture the flow physics involved in a rotor stator cavity. It has been well accepted that if G >= G_{max} (= $1.05/\mathrm{Re}_{ro}^{0.2}$), the stator does not have too much effect on the flow physics of rotor-stator cavity. So, in order to have better understanding of the wheel space cavity flow physics, the usual designs involve maintaining the above said dimensionless gap ratio in the wheel space cavity. The goal of any wheel space design is first to cool the disk, and secondly to minimize the drag component on the disk. Since the above objective involves optimizing the cooling flow as well as the wheel space cavity dimensions, the design process is an iterative procedure, and is discussed briefly in the following sections.

A cross sectional view of the engine is shown in Figure 4-1, which shows the various systems/cavities in the engine. These various systems are discussed in the following sections. The wheel space cavities are the cavities that are inbound of the inner rim seal and outbound of the hub seal. The bleed cavities are the cavities that are inbound of the outer rim seal and outbound of the inner rim seal.

4.1.1.1.2 Wheel Space Buffer Air

As mentioned in the introductory section, buffering up wheel space cavities to prevent mainstream flow ingress is a performance penalty. In order to minimize this penalty, rim seals and discourages are usually employed in the design. Owen & Phadke ran many experiments to determine the buffer flow, required to prevent mainstream gas ingress, for rim sealed disks. The various experimental configurations that were run by them are shown in Figure 4-2. These experiments were conducted to estimate the minimum buffer flow requirements for different seal arrangement within the following variable range

$$0.0025 =< G_c =< 0.04$$
$$G = 0.1, 0 =< \mathrm{Re}_{ro} < 1.2e6$$

and the minimum required buffer mass flow rate is represented by

$$\dot{m}_{min} = C_2 \mu\, r_o G_c{}^m \mathrm{Re}_{ro}{}^n \ ,$$

where the constants are dependent on the type of seal being used and is discussed by Owen & Phadke. When a mainstream flow is involved, the minimum buffer flow is dependent on the external flow Reynolds number and experiments have shown that Seal 2 of Figure 4-2 performs best in terms of reducing the ingress when external flows are present and that seal 4 of Figure 4-2 performs best, when there is no external flow.

Using the abovementioned process, the various buffer flows in the respective wheel space cavities have been calculated and is presented in Figure 4-3.

4.1.1.1.3 Thrust Balance System

The thrust balance system for the Ramgen rotor is based on the rotor itself acting as the thrust piston. The tip clearances required for the Ramgen rotor operation dictate the bearing sizes. Since small tip clearances are required for the Ramgen rotor operating, the bearing size is small, which results in low thrust capability for the bearings. As a result, an active control of the secondary system pressures in the forward and aft wheel space cavities leads to the bearings experiencing minimal axial thrust.

The Ramgen rotor operates under supersonic conditions. So the inlet is subject to unstarts which causes changes in the aerodynamic conditions in the flow path resulting in fluctuations in the axial thrust experienced at the bearings. To reduce the effect of such fluctuations on the bearings, an active control of the wheel space pressures is used.

The axial thrust on the Ramgen rotor main flow path has two components namely the thrust from the axial component of the fluid momentum and the other due to the axial component of the pressure terms, i.e.,

$$\text{Thrust} = F_{momentum} + F_{PdA}$$

$$F_{momentum} = \dot{m}\,(Vi - Ve) + PiAi + PeAe$$

where the areas are the cross sectional areas through which the fluid flows in and out, along the rotor flow path, as shown in Figure 4-4.

$$F_{PdA} = PiA_{intake} + PeA_{exhaust}$$

where the areas are the corresponding areas on the rotor surface that are in contact with the fluid, as shown in Figure 4-4.

In addition to the axial thrust generated from the rotor main flow path, axial thrust is also generated from the aft wheel space cavity. The design philosophy adopted in the Ramgen design is to overcome this overall axial thrust by pressurizing the forward wheel space cavity with adequate pressure and adjusting the same for different operating condition so that the overall thrust experienced by the bearings are not too different. This active control of pressure ensures that the changes in the axial thrust values do not exceed the thrust limit capability of the bearings.

The starting sequence for the supersonic inlet is shown in Figure 4-5. As can be seen, the inlet during the starting sequence goes from being unstarted with no backpressure to being started with no backpressure due to the bleed on the main flow path. Once the inlet is started, the back pressure is gradually increased to improve the efficiency and to simulate the real compressor environment. Beyond a certain level of increase in back pressure, the inlet becomes unstarted and a worst case axial thrust is experienced by the bearings as shown in Figure 4-6.

4.1.1.1.4 Disk Drag Calculations

The buffer air in the wheel space cavity represented in Figure 4-3 causes aerodynamic drag on the rotor, which results in a performance penalty. In order to minimize the drag on the rotor, the wheel space gap is optimized based on the many experimental works of Owen and Rogers. The following procedure has been used for estimating the disk drag.

The drag power for the rotating disk is given by $P = \tau \, \omega$, where τ is the torque and ω is the speed. This drag results in heating of the air in the wheel space cavity. Assuming that the system is adiabatic, this power is equal to the change in the enthalpy of the fluid in the disk cavity. The above assumption results in the computation of the temperature rise of the air in the disk cavity, using an iterative procedure, i.e., $\Delta h = \tau \, \omega$.

The torque of the system, τ, is evaluated using $\tau = C_{ms} \, \rho \omega^2 r_o^5 / 2$, where C_{ms} is the dimensionless friction coefficient which is got from suitable experimental data, ρ is the density of the fluid, ω is the rotational speed and r_o is the disk outer radius. Many experimentalists including Gartner W., Zimmermann, Millward, Daniels etc., have conducted experiments to determine C_{ms} for various operating conditions and suitable data from the above experiments has been used to the determine the torque of the Ramgen rotor. A typical chart depicting the trend of the C_{ms} is shown in Figure 4-7. The calculated disk drag for different rotor speeds are specified in Table 4-1.

In an effort to determine the viscous drag on the Rampressor rotor, one inlet (flowpath) was labeled in the following manner. See the attached sketches for more detail.

    Area 1 (A1) – Inlet floor
    Area 2 (A2) – Ramp floor
    Area 3 (A3) – Expansion floor
    Area 4 (A4) – Exit floor
    Area 5 (A5) – Inlet strake wall
    Area 6 and 9 (A6) (A9) – Ramp Strake Walls
    Area 7 and 10 (A7) (A10) – Expansion Strake Walls
    Area 8 (A8) – Not used due to the assumption of the normal shock at the end of the inlet
        strake
    Area 11 (A11) – Exit Strake Wall

The boundary layer drag calculations were made using the BLC2 code, modeling each area as a flat plate. Note that the boundary layer growth was not carried over to downstream areas. The effect of the shock structure would tend to compress the boundary layer. This approach gives the most conservative estimates of viscous drag.

The BLC2 code was run using a transition criterion based on $Re_\theta / M = 150$. Re_θ is the Reynolds number based on momentum thickness, and M is the Mach number. This transition criterion was chosen to insure a very short laminar boundary layer. The code only requires the plate length

and does all calculations assuming a unit width (ft). All calculations were performed with a constant step size of $\Delta x=0.1"=0.008333$ft.

The following areas have the same input parameters:

A1=A5
P = 14.7 psia = 2116.8 psfa
T=528.7 R
V=2573.7 ft/s
γ=1.4
Twall=1060 R (This is the maximum wall temperature desired per Ram Pudupatty)
M=2.28
L1=L5=0.7104 ft

A2=A6=A9

Note that the assumption was made that the series of oblique shocks on the inlet ramp do not drastically change the free-stream flow conditions. The following parameters represent approximately the average values across the ramp taken from Shawn's shock table.

P = 21.0 psia = 3024 psfa
T=586.5 R
V=2451.5 ft/s
γ=1.4
Twall=1060 R
M=2.06
L2=1.5296"=0.1275ft (ramp length assuming throat height is 0.293" and the ramp inlet height is 0.727", calculated assuming a single ramp angle with L2 as the hypotenuse)
L9=L6=1.4667"=0.122 ft

A3=A7=A10
P = 57.44 psia = 8278.56 psfa
T=810.49 R
V=1811.79 ft/s
γ=1.4
Twall=1060 R
M=1.3
L3=L7=L10= 0.875"=0.0729 ft

Note that the above length places the normal shock at the end of the inlet strake. The flow path height at the shock is 0.408", this is the assumed flow path height and strake height at the flow path exit.

A4=A11
P = 132.79 psia = 19121.76 psfa
T=977.95 R

V=766.06 ft/s
γ=1.4
Twall=1060 R
M=0.5
L4=L11=8.5"= 0.7083 ft

The code generates results in lbf/ft making it necessary to describe the width (or is some cases height) of each planar area.

W1=1.460"=0.1217 ft

Note the force calculated for area 1 is halved since the inlet flow plane is triangular.

W2=W3=1.3833"=0.1153ft

W4=1.460"=0.1217ft

Note the force calculated for area 4 is halved since the exit flow plane is triangular.

W5=0.727"=0.1217ft

Area 6 and 9 must be divided into two pieces. The top piece being a rectangle, and the bottom a triangle which neglects the area covered by the inlet ramp.

W6-top=W9-top=0.293"=0.0244 ft
W6-bottom=W9-bottom=0.434"=0.0362ft

Again, note that the force calculated for areas 6-bottom and 9-bottom is halved in order to neglect the wall area covered by the inlet ramp.

Area 7 and 10 must be divided into two pieces. The top piece being a rectangle, and the bottom a triangle which neglects the area covered by the expansion ramp.

W7-top=W10-top=0.293"=0.0244 ft
W7-bottom=W10-bottom=0.115"=0.0096ft

Again, note that the force calculated for areas 7-bottom and 10-bottom is halved in order to neglect the wall area covered by the expansion ramp.

W11=0.408"=0.0340ft

The results are shown in Table 4-2.

Taking the current Ramgen engine concept with a mean flow radius of 4.44" or 0.37 ft with constant 54872 rpm and 3 flowpaths, one can arrive at the additional motor power that will be required due to the viscous drag.

$$P = 3 * 3.026 lbf * 0.37 ft * \frac{2\pi}{60} * 54872 rpm$$

$$= 19300.6 \frac{lbf \cdot ft}{s} = 35.1 hp$$

The numbers for the boundary layer drag have been re-worked using the updated flow paths and conditions from Shawn. The results are given below:

AR = 1.5
Drag = 3.987 lbf per flow path or 11.961 lbf for the entire disk.
Rcl = 4.44 in
RPM=49036.8
Power loss due to drag = 41.3 hp

AR = 2.2
Drag = 3.869 lbf per flow path or 11.607 lbf for the entire disk.
Rcl = 5.375 in
RPM=40506.7
Power loss due to drag = 40.1 hp

For the previous case run which was I believe an AR=2.0 the results were as follows:

Drag = 3.026 lbf per flow path or 9.078 lbf for the entire disk.
Rcl = 4.44 in
RPM=54872
Power loss due to drag = 35.1 hp

Conclusions

The two new aspect ratios have increased the wheel drag, although not significantly. The reason for the larger drag in the AR=1.5 case is due to the increased strake height resulting in increased viscous drag although this effect is very small in comparison to AR = 2.2. The drag power requirement is further increased by the increased rotation rate in the AR=1.5 case.

4.1.1.1.5 Thrust Loading

In order to investigate the potential operating conditions of the Rampressor the following physical flow conditions were identified:

1) Un-started with minimum back pressure - The flow in this condition is characterized by a normal shock at the rotor inlet, the flow would then accelerate to sonic conditions at the flowpath throat, finally expanding supersonically to the rotor exit.

2) Started with minimum back pressure - The flow in this condition would include all of the oblique shock structure at the inlet ramp, but no normal shock was assumed to form after the flowpath throat causing the flow to expand supersonically to the rotor flowpath exit.

3) Started with maximum back pressure - This condition represents the flowpath inlet operating on design with the oblique shock structure on the ramp incline flowed by a normal shock after the rotor throat.

4) Un-started with maximum back pressure – This condition like condition 1) is characterized by a normal shock at the flowpath inlet prior to the ramp, the flow is then assumed to accelerate to nearly sonic conditions (i.e., M=0.9) at the throat and then expand subsonically to the rotor exit.

Of the four conditions 3) and 4) represent the most extreme thrust loads on the rotor due in part to the large PdA forces created by the high back pressure.

4.1.1.1.6 Seal Design and Analysis

Figure 4-1 indicates that the Ramgen rotor contains both the rim as well as the hub seals. The double shrouded seal on both the forward and the aft sides of the disk is to create a) a separate bleed cavity pocket for the bleed flow that is bled from the main flow path so that an individual control on the pressure exists in that cavity providing control over the mass flow rate of air being bled from the main flow path and b) to have individual control of the pressure in the wheel space cavity which would provide separate control of the axial thrust in the system. For the hub seals a four tooth straight through seal is used, where as for the double shrouded rim seals, a two tooth step seal is used to minimize the leakage into the bleed cavity and thus reduce the performance penalty on the engine. The radial clearances at hot running conditions for these seals are set at 0.005 inches. The leakages estimated for these different seals are presented in Table attached along with Figure 4-8. The seal flow rates are computed based on the work of several investigators including Zimmermann, Rhode, Vermes, Wittig, etc. These above mentioned authors have conducted sealing experiments and have varied many different design parameters to predict the seal leakage mass flow rates under various operating conditions. Typically the seal flow rates are expressed using the following equation,

$$\frac{\dot{m}_s \sqrt{T_{t1}}}{AP_{t1}} = \frac{C_1 C_d \beta}{\sqrt{R(1-\alpha)}}$$

where,

$\dot{m}_s$ = seal mass flow rate, lb_m/s.
β = fn(P_{t1}/P_{s2},Number of teeth)
α = fn(Pitch between teeth, Tooth Width, Clearance)
C_d = fn(Number of teeth, Type of seal)
A = leakage area, in2
P_{t1} = upstream total pressure, psia

T_{t1} = upstream total temperature, °R

The seal leakage flows allocated without the bleed flow is shown in Figure 4-8.

4.1.1.1.7   Bleed Cavities

Boundary layer bleed and starting bleed is provided on the rotor hub to provide for more stable operation of the Rampressor. Starting bleed is planned for in order to allow each inlet on the rotor to swallow the normal shock leading to the most efficient pressure recovery and operation of the rotation inlets.

The bleed cavities are the shown in Figure 4-1. The requirement for these cavities, as stated before, is to provide individual control for the bleed flows from the mainstream flow. Since the supersonic inlet requires independent control for the bleed flows, the bleed cavities are designed to provide that flexibility. The seals on the outer and inner radii of the bleed cavities isolate the cavities (as much as possible) from the influence of the thrust balance wheel space cavity and from the mainstream flow. The bleed flows from the mainstream flow are bled using a vacuum source that is connected to the static part of the rig. Since individual valves are fitted for these separate bleed flow lines, the bleed cavities can be controlled to different flow conditions, thus providing flexibility for bleed of the boundary layer flow. The details of the bleed flows and geometries will be addressed in a later report.

4.2   Mechanical Design CDR

The work performed during this reporting period focused on the conceptual design of the test rig stationary hardware, culminating in a Conceptual Design Review. The Core Rig stationary hardware was broken down into various systems, each with an associated list of required performance characteristics, aerodynamic and/or mechanical. These systems are as follows (see also Figure 4-9):

Stationary Primary Flowpath
- Inlet Manifold
- Inlet
- Inlet Guide Vane (IGV)
- IGV/Rotor Space
- Tip Ring
- Diffuser Cascade
- Exhaust
- Exhaust Manifold

Stationary Secondary Flowpath
- Forward Disk Cavity
- Aft Disk Cavity
- Bearing System
- Thrust Balance System

Aerodynamic and Mechanical requirements for each system and the subsequent design are detailed in the following sections. The listed systems were reviewed at CDR by outside consultants with a focus on design and manufacturing issues. Comments made at CDR related to the Mechanical Design are included in the following sections.

4.2.1   Stationary Primary Flow Path Systems

4.2.1.1   Inlet Guide Vane

A single inlet guide vane was planned for at the inlet to the Rampressor rotor to turn the flow favorably onto the rotor and achieve the desired supersonic inlet flow. The need to decrease the rotor speed required a relatively high IGV exit Mach number which was pushed to about M=0.75. Preliminary design of the IGVs had not commenced until after BP3.

Aerodynamic Requirement(s):
  • Potential for Variable Geometry
  • Minimize Wake Distortion
  • Minimize Pressure Loss

Mechanical Requirement(s):
  • None

The requirement for variable geometry on the IGV is still under debate in the Aero Group, so said requirement was not addressed in the conceptual design of the rig due to the complexity of such a system. However, the mechanical design has incorporated features to easily remove and replace the IGV's in order to expedite testing of various geometries. The other listed aerodynamic requirements involve detail airfoil design and will be addressed during the preliminary design phase of the IGV.

CDR Comments:
  • Concern about complexity of variable geometry.
  • Concern about amount of turning required in single IGV stage. Suggested "double-row" IGV.

4.2.1.2   IGV/Rotor Space & "Shock Trap"

Aerodynamic Requirement(s):
  • Potential for End-Wall Bleed
  • Shock Trap

Mechanical Requirement(s):
  • None

In order to minimize distortion of the flow going into the rotating inlet, it may be required to bleed boundary layer from the end-walls upstream of the rotor and downstream of the IGV's. In addition, it is a certainty that the rotating inlet will unstart during "full-load" operation, sending a

strong pressure pulse upstream. In order to avoid damage to the upstream flow components (i.e., IGV's, Inlet Manifold, etc.), a shock trap must be incorporated into the design. As concepted, the shock trap consists of holes (or slots) in the inner and outer main air flow path, downstream of the IGV's. These holes exhaust into a plenum that will allow the shock pressure to dissipate, preventing it from propagating upstream (see Figure 4-10).

4.2.1.3 Tip Ring

Aerodynamic Requirement(s):
- Minimize Tip Clearance
- Potential to Bleed Case to Remove Boundary Layer

Mechanical Requirement(s):
- Primary Containment

For the inlet to achieve maximum performance, tip leakage must be controlled to the greatest extent possible. A major contributor to tip leakage is tip clearance. Therefore, the tip ring is required to provide minimum clearance with the strakes at steady state operation. To achieve this, the current concept has the tip ring as a separate component, isolating it from the surrounding structure (see Figure 4-9). The ring is held concentric to the strake tips by a pattern of circumferential pins, free to grow radially. In this way, the radial displacement of the tip ring is not influenced by the surrounding components. It may be required to heat and/or cool the tip ring during transient operation to produce minimum tip clearance at steady state. The current concept allows for this requirement, which will be determined in the preliminary design phase. The potential requirement for case bleed would drastically complicate the design of the tip ring. Further study is needed to determine the necessity of case bleed; hence the issue was not addressed in the conceptual design.

The tip ring will also be sized to provide primary containment of the rotor should a catastrophic failure occur. The ring thickness required for containment will be addressed in the preliminary design phase.

4.2.1.4 Inlet Manifold

Aerodynamic Requirement(s):
- Potential for negative pressure loading should testing require sub-atmospheric inlet conditions.

Mechanical Requirement(s):
- Connect from Facility Main Air Supply to Air Inlet.

The Air Inlet Manifold was considered in the Conceptual Design as a radial style inlet typically found on an Industrial Gas Turbine installation. However, the requirement for potential sub-atmospheric pressures would necessitate a mechanically sound inlet, of greater integrity than a typical sheet-metal construction. The Air Inlet Manifold will be considered in greater detail as the aerodynamic requirements become more firm and facility definition becomes available.

CDR Comments:
- No pertinent issues.

4.2.1.5   Inlet

The conceptual inlet was planned to be radial, however concerned was raised about the level of risk this imposed on the project. An axial inlet was suggested to decrease system risk which is the current plan of the Rampressor development team.

Aerodynamic Requirement(s):
- Minimal Pressure Loss
- Minimal Flow Distortion

Mechanical Requirement(s):
- Structural Link between Bearing and Rig Mounts
- Provide Flow and Oil Passages for Secondary Systems

The Air Inlet has been concepted to meet the above-mentioned aerodynamic requirements using rule of thumb guidelines for flow turning and placing blockages in the flow. The flow path will be finalized by the Aero group during the preliminary design phase. As currently concepted, the air inlet will provide access to all of the forward secondary flow systems, including wheel space buffer flows, boundary layer bleed suction flow and oil flow (see Figure 4-9). The inlet will be a weldment made up of easily fabricated details in order to minimize fabrication lead times and cost. Follow on rotordynamics work will verify the structural stiffness of the inlet.

CDR Comments:
- Reiterated need for "clean" airflow into Inlet Guide Vane.
- Suggested Axial Inlet (vs. Radial) for cleaner flow.

4.2.1.6   Diffuser Cascade

Aerodynamic Requirement(s):
- No Current Requirement

Mechanical Requirement(s):
- None

It has been determined by the Aero Group that a Diffuser Cascade downstream of the rotor exit is not required for this test program.

CDR Comments:
- Agreed with conclusion of no Diffuser Cascade.

4.2.1.7 Exhaust

Aerodynamic Requirement(s):
- Minimize Uncontrolled System Back Pressure
- Maximize Pressure Recovery

Mechanical Requirement(s):
- Structural Link between Bearing and Rig Mounts
- Provide Flow and Oil Passages for Secondary Systems

The Exhaust has been concepted to meet the above-mentioned aerodynamic requirements using rule of thumb guidelines for diffusion and pressure recovery. It has been sized to give twice the required outflow area to avoid unwanted, uncontrolled backpressure in the system. The flow path will be finalized by the Aero Group during the preliminary design phase. The current concept is for the exhaust to be manufactured in two (2) separate pieces, joined together as an inseparable assembly after machining of the flowpath (see Figure 4-9). The Exhaust will provide access to all of the aft secondary flow systems, including wheel space buffer flows and oil flow (see Figure 4-9). Follow on rotordynamics work will verify the structural stiffness of the exhaust.

4.2.1.8 Exhaust Manifold

Aerodynamic Requirement(s):
- Minimize Uncontrolled System Back Pressure
- Maximize Pressure Recovery
- Capability to Control Back Pressure of System

Mechanical Requirement(s):
- Connect to Facility Exhaust

The Exhaust Manifold has been concepted to meet the above-mentioned aerodynamic requirements using rule of thumb guidelines for pressure drop across flow interfaces. It has been sized to give twice the required outflow area to avoid unwanted, uncontrolled backpressure in the system. A valve will be placed on the exhaust outlet to allow control of system backpressure during rig testing. Connection to the facility exhaust should be straightforward and will be addressed as facility definition becomes available.

CDR Comments:
- Reiterated need to avoid uncontrolled backpressure of system.

4.2.2 Stationary Secondary Flow Path Systems

4.2.2.1 Bearing System

No Aero comments here.

4.2.2.2   Forward Disk Cavity

Aerodynamic Requirements(s):
- Remove Disk Flow Path Bleed Flow (Vacuum)
- No Secondary Flow leakage into the Main Air Flow Path

Mechanical Requirement(s):
- Provide Disk Cavity Buffer Flow to mitigate Disk Drag and Heating
- Provide Bearing Seal Buffer Flow
- Provide Disk Cavity Buffer Flow
- Function as Thrust Piston for Thrust Balance System (addressed in Section 4.1.2.2.4, below)

The Forward Disk Cavity (see Figure 4-11) performs several functions crucial to the operation of the rig. As concepted, Disk Flow Path Bleed Flow will be removed from a plenum created by the interface of two sets of labyrinth teeth on the disk and corresponding static surfaces on the Forward Case. Negative pressure (vacuum) will be applied to this plenum to meet the pressure differential required to bleed the rotating inlet. This negative differential will also serve to meet the aerodynamic requirement of no leakage into the main air flow path. Flow passages in the Forward Case have been sized to accommodate the flows based on preliminary bleed flow estimates. The concept also allows for purge air flow for the cavity as well as buffer flows for the pertinent seals.

CDR Comments:
- Concerned about Disk Buffer Flow and Bearing Seal Buffer Flow feeding from the same cavity due to potential for over-pressurizing sump if Bearing Seal damage occurs. Suggested giving Bearing Seal independent feed cavity. Ramgen will implement in Preliminary Design.

4.2.2.3   Aft Disk Cavity

Aerodynamic Requirements(s):
- Remove Disk Flow Path Bleed Flow (Vacuum)
- No Secondary Flow leakage into the Main Air Flow Path

Mechanical Requirement(s):
- Provide Disk Cavity Buffer Flow to mitigate Disk Drag and Heating
- Provide Bearing Seal Buffer Flow
- Provide Disk Cavity Buffer Flow

The Aft Disk Cavity (see Figure 4-12) performs functions similar to the Forward Disk Cavity. However, there is no requirement for the removal of Bleed Flow, which will be exhausted exclusively on the forward side of the disk. The same requirement for flow path leakage (i.e., no leakage into the Main Air Flow Path) applies to the aft disk cavity. In this case, a relatively low pressure off take is provided to dump leakage from the Main Air Flow Path through the outboard seal, and from the inboard seal, overboard.

4.2.2.4   Thrust Balance System

Aerodynamic Requirements(s):
  • None

Mechanical Requirement(s):
  • Provide Balancing Force against Aerodynamic Loading due to Differential Pressure across Rotating Inlet.

The Thrust Balance System is required to offset the aerodynamic loading of the disk, as well as the pressure required in the aft disk cavity for disk buffering. Without the Thrust Balance System, the rolling element bearings in the rig would fail due to overload. As currently concepted, the Thrust Balance System utilizes pressurized forward disk buffer flow (see Section 4.1.1.1.5) acting on the forward face of the disk to combat the pressures acting on the aft side of the disk (see Figure 4-13). The pressures in the disk cavities will be regulated in order to maintain thrust on the bearings within design limits.

4.2.3   Test Rig Rotor Cartridge Design

4.2.3.1   Aerodynamic/Heat Transfer Design and Analysis

4.2.3.1.1   Summary

This section summarizes the results of the preliminary rotor thermal analysis for the compressor test rig. The finite element modeling performed in ANSYS included analyses on a 2D axisymmetric model and two different 3D sector models. Both steady state as well as transient runs has been completed. The two 3D models correspond to the two different disk shapes that Ramgen has come up with, to-date, for 105,000 rpm disk. The design goals of the disk are to maintain the peak temperatures in the disk at around 450 °F and the corresponding bulk temperatures below 400 °F at full load steady state conditions. The region that is subject to the highest temperature in the disk is the aft face of the disk, in the region above the rim seals. In order to reduce the temperatures at the rim, the design philosophy includes impingement cooling of the rim on the aft side of the disk, for the 105,000 rpm disk. All the analyses assume a rotor of around 6 inches diameter. A more sophisticated analysis will be performed in future once all the performance studies have been completed.

4.2.3.1.2   Introduction

The two disk shapes analyzed are based on the designs that were optimized using ANSYS. All the thermal boundary conditions for these models have been evaluated assuming that the rotor spins at 105,000 RPM. For this preliminary work, no bleed holes in flow path have been considered.

The 2D axisymmetric model is got from the optimization run performed by ANSYS and is shown in Figure 4-14. The thermal boundary condition for which this analysis has been completed corresponds to conditions existing in the rotating diffuser downstream of the ramp.

The two 3D models on which both the steady state as well as transient thermal analyses were performed are shown in Figure 4-15 and Figure 4-16 and were obtained from the optimization runs using ANSYS.

4.2.3.1.3   Modeling Assumptions

The boundary conditions applied to the finite element models were on the forward and aft disk faces, the forward and aft rim seal surfaces, the floor and the strakes of the flow path. The boundary conditions on the disk faces were varied in the radial direction and fluid elements were used in all the models to calculate the heat pick up in the models. The bulk temperatures for the forced convection heat load on the disk faces were calculated based on the adiabatic wall temperature, assuming that the fluid core in the wheel space cavity rotated at a certain velocity. This assumption is standard practice in the gas turbine industry for wheel space cavity flows.

Also, for all these analyses, the wheel space gap (S) to the rim radius (Ro) ratio (S/Ro) has been maintained at 0.10. It has been recommended by many authors who have studied this subject extensively (refer section 4.1) that this ratio needs to be only around 0.03-0.04, but not enough data is available in the open literature to support one way or the other. A relevant calculation revealed that either of these two ratios would be large enough to ensure that the boundary layers on the rotor and the stator surfaces remain separate and do not affect each other. This basically means that the correlations used for evaluating heat transfer boundary conditions for the current models (i.e., S/Ro ~0.10) should be a good representation for the S/Ro of ~0.03 and the results of these finite element models can be used as a first cut for temperature profiles.

A detailed explanation about the boundary conditions applied to these finite element models is deferred until a sophisticated analysis is performed in future.

4.2.3.1.4   Analysis & Results

Figure 4-17 through Figure 4-23 show some of the steady state and transient temperature profiles for the rotor. For all the analyses the inlet conditions for the disk cooling flow / buffer flow has been maintained at conditions specified in section 4.1 in the forward and aft disk cavities, to meet the full load steady state design objectives. In addition, the rim on the aft disk face is cooled by impingement with 0.05 lbm/s, 120 psia, and 300 °F air. As was mentioned earlier, the wheel space cavities are assumed to have a fluid core rotating at a certain speed (based on standard gas turbine industry practice). Since the data available in the open literature is not exhaustive and does not cover the Ramgen rotor conditions at 105000 rpm, a conservative approach on the flows have been followed. Based on test data that Ramgen generates, the above-mentioned flows will be tailored to suit our needs.

For the transient runs, the rotor is assumed to operate from 0 RPM to 105000 RPM in 5 minutes, and the rotor remains at that particular operating condition for 55 additional minutes. The

boundary conditions applied to the model reflect the above mentioned start cycle, and has been scaled linearly for these analyses, which is considered as a reasonable assumption at this stage. A more detailed look at how the boundary condition varies with speed etc., will be addressed in future once additional details become available.

Figure 4-17, Figure 4-19, Figure 4-20, Figure 4-22 and Figure 4-23 show the steady state temperature profiles for both the 2D as well as the 3D models. Figure 4-18, Figure 4-21, Figure 4-24, Figure 4-25, Figure 4-26 and Figure 4-27 show the transient temperature profiles for the above mentioned finite element models at different locations. All temperatures are shown in °F and the time is typically expressed in fractions of hours. In these figures the time required for the disk to reach full thermal soak for the assumed boundary conditions is shown. It is important to note that this particular time is a function of the disk thickness as well as the assumed boundary conditions, especially the ramping schedule from 0 RPM to 105000RPM. Since Ramgen has not yet decided on the final rig start sequence, as mentioned earlier, the simplest start sequence has been assumed for these analyses. For the above-mentioned start sequence, depending on the disk design, the time taken for the rotor to be completely thermal soaked can be anywhere between 10 minutes (Figure 4-24) and 25 minutes (Figure 4-18 and Figure 4-21).

4.2.3.1.5 Conclusion

A preliminary thermal analysis of the 6 inch rotor for the Ramgen compressor rig was completed. Both steady state and transient analysis have been performed so that a better estimate of the structural analysis can be carried out. The discussed results are preliminary and a more sophisticated analysis will be carried out in future, once additional details are available.

4.2.3.2 Rotor Mechanical Design

This report documents the progress achieved towards the mechanical design of the Rampressor rotor during the period 03/2002 – 09/2002. Three aero design rotor candidates have been analyzed to date. The 105,000 rpm design with a pressure ratio of 16:1, a 40507 rpm design with a 11:1 pressure ratio and a 49000 rpm design with a 15:1 pressure ratio. The results of these design iterations were used to understand the mechanical design challenges and to help narrow the design space and at the same time, meet the overall Rampressor design requirements. The following sections will outline the rotor design requirements and also present the design methodology used to design and analyze each of the design iterations. The results presented will not cover all the details of each of the design iterations, and are only intended to give a flavor of the approach and the design challenges.

4.2.3.2.1 Vibration Requirements

Blades and disks in gas turbine engine have always been prone to fatigue problems, generally due to the blade flexural / torsional natural modes of motion or disk excitation which produces excessive vibratory stress levels. Vibration related cracks and separations are prime source of unplanned engine shutdown. Limiting the vibratory stress levels prevents vibration related cracks and potential strake/disk separation. It is desirable to have the fundamental frequency to be above 3/rev to avoid excitation by inlet distortion and provide a strake with reasonable

stiffness. Any upstream and downstream excitation orders should also be avoided. Historically, +/- 15 ksi vibratory margin is achieved by keeping the steady state stresses less than 80 percent of 0.2 percent material yield at temperature and keeping the peak vibratory stress locations away from maximum steady state stress location.

4.2.3.2.2 Life Requirements

This design criterion is to ensure that the calculated LCF life exceeds the design requirements for all components that are cyclically loaded by normal engine operation. Insufficient margin results in initial service lives below customer expectations and possible disk/rim separations. The desirable life requirements for the Rampressor are 10,000 LCF cycles and with $1x10^7$ cycles of HCF life. The stresses in the Rampressor disk should be acceptable to meet the HCF and LCF concerns. Ramgen design practice requires the equivalent stress in the rotor to be less than 80 percent of 0.2% YS of the material and the principal stress to be less than 80 % of the UTS. The allowable vibratory (alternating) stress margin reduces as the mean stress in the strakes increases. The Goodman diagram for Titanium suggests that the vibratory stress margin is to be less than 10 ksi if the mean stress is greater than 100 ksi. Also, the location of the peak alternating stress in the strake should not coincide with the location of the peak static stress.

4.2.3.2.3 Burst Requirements

The traditional method for calculating the burst speed margin of a turbine rotor has been the use of an equation relating the component average tangential stress to the material ultimate strength.

$$\text{Burst Speed margin} = \sqrt{(MUF * UTS / ATS)}$$

where,
    MUF = material utilization factor, typically used value is 0.85 for tangential burst ratio.
    UTS = -3σ minimum UTS at the component maximum average bulk temp.
    ATS = Average Tangential stress at design speed.

The design intent is to have a 20 percent burst margin over the operating speed to provide a safe margin on hub burst. The requirement for adequate burst margin stems from the safety hazard involved if an uncontained failure occurs. The basic disk average tangential and radial stresses must be low enough to provide this margin. The average radial stress is calculated at different radii and the highest of these values is considered for radial burst calculations.

4.2.3.3 Mechanical Design Methodology

The first step was to decide on a material that would best meet the design requirements for the Rampressor rotor. The shape of the disk was optimized in 2D and the outline of the disk was transferred to UG to develop the solid model. To validate the 2D analysis, no bleed features were modeled. Typically the 2D and 3D models gave very similar stress distributions. The 3D models were used to evaluate the stress distribution in the part.

4.2.3.3.1 Material Selection

An extensive material selection study has been carried out. Some of the candidate materials considered were C450, AL354, DP718, Ti 64, Ti 6242 and Ti 6246. The bulk temperature of the rotor was estimated to be around 200F and the stress and weight requirements lead to a Titanium rotor. Titanium has a strength-to-weight that is 40% better than any other conventional material. In temperature regions less than 600F, annealed Ti-6Al-2V-4Zr-2Mo has shown proven durability, is easy to machine and work and generally trouble free. It has also a very good corrosion and erosion resistance. Ti-6Al-2V-4Zr-6Mo has higher strength and ductility than Ti-6Al-2V-4Zr-2Mo, but inferior notch sensitivity. The -3σ YS @ 200F =106 ksi, and the -3σ UTS @ 200F = 115 ksi. Figure 4-28 shows the variation of mechanical strength properties of Ti-6Al-2V-4Zr-2Mo with temperature.

4.2.3.3.2 Disk Optimization

The rotor was analyzed in ANSYS 6.1 using 2D, 3D and 2D/3D modeling approaches. The stress and deflection components (i.e., radial, tangential and axial) were monitored. The basic design approach was to minimize the deflections and stress to have a robust design that would meet the aerodynamic requirements. The ANSYS optimizer was used to minimize the background stresses in regions having bleed holes as well as keeping stresses in webs and at disk bore to less than 100 ksi to meet the LCF requirements.

4.2.3.3.2.1 2D Disk Shape Optimization and Analysis

The basic 2D axisymmetric shape of the disk was developed in Ansys using the APDL toolbox. The shape of the disk is parameterized using design variables like the coordinates of 'keypoints'. Curves or lines can be developed based on these 'keypoints'. Areas can be developed to enclose the lines. This area would represent the axisymmetric hoop-carrying portion of the Rampressor Disk. For optimizing the disk shape two approaches were followed: Approach 1. The weight of the ramp above a pre-determined radius was modeled as a point mass lumped at the C.G of the ramp to model the pull force from the rim, the weight having been estimated from a solid model of the ramp area. Approach 2. The flowpath was modeled completely. Figure 4-29 illustrates the first approach. The optimizer performs a series of analysis-evaluation-modification cycles. That is, an analysis of the initial design is performed, the results are evaluated against specified design criteria, and the design is modified as necessary. This process is repeated until all specified criteria are met. The objective of the optimization was to determine the minimum-weight disk to meet all our design objectives. Design Variables (DVs) are independent quantities that are varied in order to achieve the optimum design. Upper and lower limits are specified to serve as "constraints" on the design variables. These limits define the range of variation for the DV. The coordinates of the keypoints are the DVs for the present optimization. State Variables (SVs) are quantities that constrain the design. They are also known as "dependent variables," and are typically response quantities that are functions of the design variables. The burst ratio margin (radial and tangential) of the disk, the peak stress on the bore and the faces of the disk are the SVs. The objective function is typically the weight of the rotor. The best design is the one that satisfies all constraints and produces the minimum objective function value. The disk shapes were analyzed for a number of different design iterations.

PLANE42 elements to determine the stress distribution in the disk. The "thickness option" was used to simulate the non-hoop carrying regions on the rim of the disk. Figure 4-30 shows some of the typical shapes that the optimizer analyzes before arriving at an optimized shape. Once the disk shape has been optimized it is merged with the flow path shape to complete the disk. Figure 4-31 presents results of a typical analysis. A radial distribution of temperature (150-530F) was applied to the disk. The equivalent stress (or von mises stress) peaks at the bore of the disk. The principal stress peaks at the neck of the disk. The principal stress equals the radial stress in the neck region and is equal to the hoop stress in the bore. Figure 4-32 through Figure 4-33 show the results for the 2.2 aspect ratio, 40,507 rpm case. The stress results can be scaled for the 30,900 rpm case (assuming the same temperature distribution). The Rampressor disk is to have a number of bleed passages requirements for starting, performance and boundary layer bleed. A detailed 3D model is to be used to better predict the stress distribution. To help optimize the placement and the size of the cross holes a number of parametric tools were developed to minimize the geometric stress concentration factor (K_t) that is to be expected.

4.2.3.3.2.2 3D Stress Analysis

Once the optimized disk shape is analyzed, a 3d model was developed in UG-17 and the geometry was transferred back to ANSYS using parasolids. A 120-degree sector model was used for cyclic symmetry stress analysis. Care should be taken to ensure that the left and right wedge faces are of the same area. CPs were used to couple these faces in all degrees of freedom. Ten noded tetrahedral structural solids were used to mesh the solid. Smart sizing was used to get a good quality mesh. Mesh 200 elements were used to 'seed' the left and right faces to ensure similar meshed on the cyclically symmetric faces. A radial temperature distribution was used to replicate the disk metal operating temperatures. The nodes at the axis of rotation were constrained axially. The 3D analysis was performed for all the design iterations. A typical 3D model could have 400,000 elements. For some of the initial design iterations the solid model did not have any bleed passages defined. Figure 4-37 shows a typical 120-degree wedge model of the rotor without any bleed passages defined. A good correlation was obtained between the 2D and 3D stress models. Figure 4-38 and Figure 4-39 shows the stress distribution for the 3D model. In the interest of a faster turn around a 2D/3D stress analysis was also used. The modulus of elasticity and the density of the 3d solid that mates with the 2d disk are multiplied by a factor of three. Figure 4-40 shows the model. An early attempt was made to understand the K_t effects due to these bleed passages. The sub-modeling approach was used to predict the stresses in these features. Displacements were mapped from the full models to get a more refined stress results. A kt of 4~5 was calculated at each of the locations. This would help in dimensioning some of the features on the disk.

4.3   Test Cell Adaptor Design

The "Test Cell Adaptor" consists of all of those systems required to interface with the test cell. These include instrumentation, data acquisition, main air, lube, skid, controls, and secondary fluid systems. The final configuration and design of these system is dependent upon the facility chose to perform the testing. A listing of the facilities considered included:

- Boeing – Seattle

- Boeing – Other (Santa Sousahnna/St. Louis)
- Aerojet
- Concepts NREC
- AFRL East
- AEDC
- NASA Glenn
- NAWC China Lake
- Aero Systems Engineering
- R.R.-Alison
- Florida turbine technologies
- Honeywell ASETS
- NRC
- Atlas-Copco
- CAT Tech Center (Peoria)
- Solar
- Williams International
- Westinghouse
- PW-Canada (We will cover East Hartford)
- Pratt and Whitney, East Hartford CT
- GE
- Rocketdyne (Boeing)
- Sundstrand (San Diego)

Each of these candidates were initially contacted and were down-selected to Boeing Seattle, Aero Systems Engineering, Concepts NREC, and NAWC China Lake based on the following considerations:

- Location
- Weekly Cost
- Availability
- Drive Type
- Air Capability
- Test/Recharge Time
- Bump Risk
- Instrumentation
- Compressor Expertise

A test requirements document was composed and sent to each facility for further discussions.

4.3.1   Instrumentation

Instrumentation of the Rampressor test rig is a key component to the program since the accurate measurement of performance is a requirement. Three measurement categories were developed as well as a list of challenges and an overall instrumentation plan (see Figure 4-43). A preliminary list of vendors who are capable of installing the instrumentation into the compressor test rig was determined to be:

- ISI
- Concepts NREC
- Aerodyne
- Boeing Test Services
- Test Devices

Preliminary assembly drawings were annotated with instrumentation requirements, a sample of which is shown in Figure 4-44, to which the candidates provided ROM estimates of the instrumentation cost.

4.3.1.1 Measurement Categories

- Performance Measurements
  - Measurements For Input To Analysis Which Produces High Level Technical Goals/Objectives
- Diagnostic Measurements
  - Measurements Focused On Troubleshooting
  - Rig Aero, Rig Mechanical, Peripheral
- Control Measurements
  - Control System Required Measurements

4.3.1.2 Specific Measurement Challenges

- Device Compression Efficiency
  - Accurate, traceable, industry standard acceptable
- Rotor Pressures - How to measure:
  - rotor surface
  - case wall
  - bleed pockets (high & low freq.)
- Strake Tip Clearance/Gap: Options for our situation
- Inflow Conditions:
  - either side of IGVs
  - distortion, profiles, flow vectors, performance-related
  - (high & low freq.)
- Outflow Conditions:
  - high swirl @ M~0.9
  - distortion, profiles, flow vectors, performance-related (high & low freq.)
- Mechanical Instrumentation:
  - rpm, rotor axial position, strake flutter
- Various Mass Flows:
  - seal leakage, strake leakage, & bleed mass flows
- Other: TBD

4.3.1.3 Instrumentation Strategy

- Ramgen preliminary instrument package development
  – Internal measurement planning and Identification of areas for improvement
  – Phase 1-3 RFQ release
  – Preliminary instrumentation plan
- Phase 1A - External review of measurements and techniques
  – Comment on measurement and control methodology
  – Specific instrumentation and technique recommendations
  – Specific controls and hardware recommendations
- Phase 1B - Ramgen core rig instrumentation package development
  – External response integration and final instrument selection
  – Preliminary Instrument routing plan
  – Acquisition methodology
  – Manufacturing prioritization and schedule development
- Phase 2 - Turnkey or Distributed Fabrication
  – Instrument fabrication
  – Instrument final routing plan
  – Hardware modification to routing plan
- Phase 3 - Instrument installation and check out
  – Final Instrument routing
  – Preliminary Instrument check-out

4.3.2 Controls

The controls system is envisioned to either utilize the controls capabilities available at the as yet to be determined test facility or the controls used for the Tacoma Ramgen Engine testing.

4.3.3 Lube

The lube system is envisioned as being a self-contained unit mounted on a lube skid that will be placed near the rig skid. The lube system will supply the lubrication for the rig only as the drive unit will have its own independent lubrication system.

- Lube systems for compressor rig and drive separate
- Flow rate for thrust bearing is TBD
- Thrust Bearings will contaminate oil quickly
- High speed bearings will have to be highly filtered
- System dependant of flow rates and facility conditions

4.3.4 Drive

The general requirements for the Rampressor drive system were determined to be as the following:

- 1125 Horse Power at maximum speed
- 40,000 to 49,000 RPM Range maximum
- Independent Mist Lube System

- Full Control Package
  1. Ramp Capable
  2. Over-Speed Protection
  3. Full Interface capable

Drives considered included electric, steam, gas turbine, and pneumatic types. A Barbour Stockwell Inc. (BSi) air expander turbine was selected from several technology candidates. The drive power (kW) vs. speed (RPM) is shown in Figure 4-45.

Drive power is calculated along with rotor thrust, Table 4-3 shows the estimates of drive power that were made using control volume analysis. Drive power was calculated for the other rotor operating conditions outlined in previous sections, however the largest power requirements are represented in Table 4-3.

4.3.5 Main Air Systems

The main air systems are defined as those systems required to route air to and from the "core" rig. This includes the air supply piping as well as any exhaust piping. These systems will be very dependent upon the test facility.

4.3.6 Secondary Fluid Systems

The secondary fluid systems are those other systems such as:

- Bleed exhaust (vacuum) lines
- Wheel space purge supply and exhaust lines
- Thrust balance air lines

4.3.7 Skid

The skid is conceptually intended to be an elevated table or frame that supports both the Rampressor and drive system as well as hold the lube, controls, instrumentation sensors, and control valves. This is intended to make shipping and installation of the test rig less difficult.

4.3.8 Analog to Digital Converters

The analog to digital converters (otherwise known as the A/D system) is required to digitize and record the data from the test. The types of data correspond to that spelled out in the instrumentation, but there are various types of signals that need to be recorded that have requirements such as:

- Acquisition Rate: 1 Hz to 1MHz
- Signal Type: RTD, Thermocouple, milliamp, VDC
- Measurement Type: Pressures, Temperatures, Rotation Rates, Vibration, Rotor Tip Clearance, Bearing Thrust Force, etc.
- Channel Count: Single channels to 100's of pressure channels
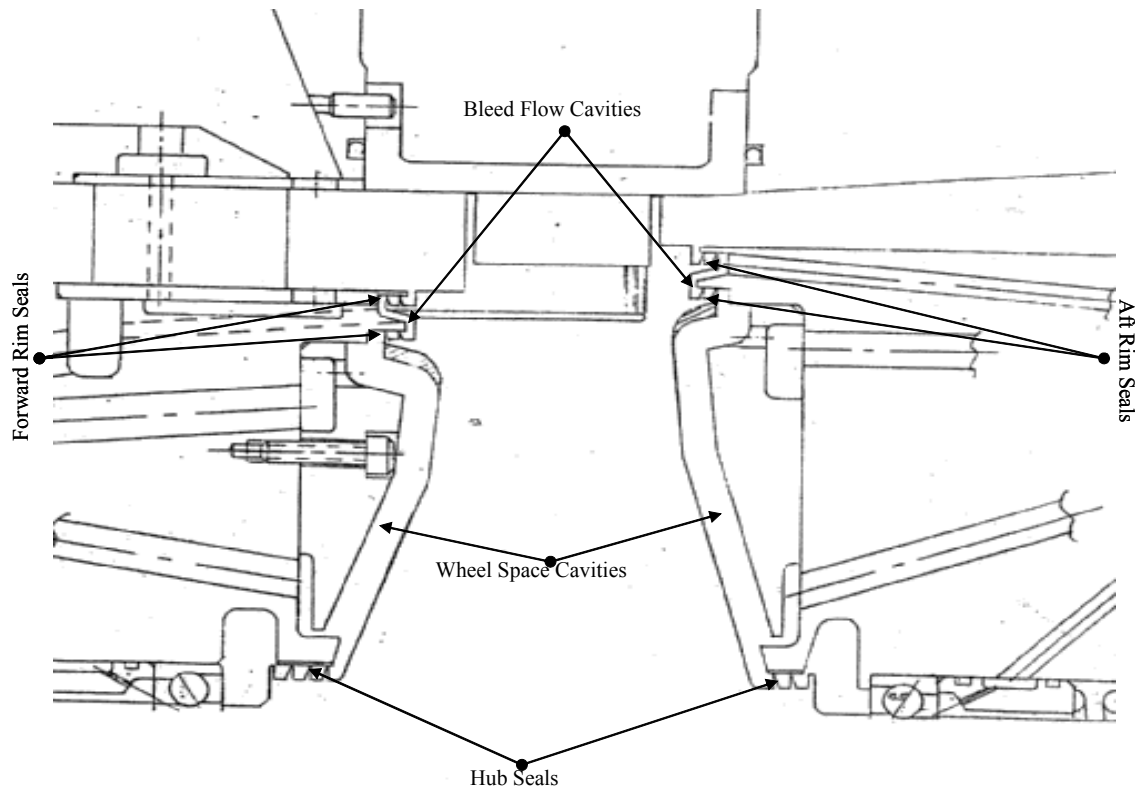
Figure 4-1   Cross section of the Ramgen Rotor Flow Path.
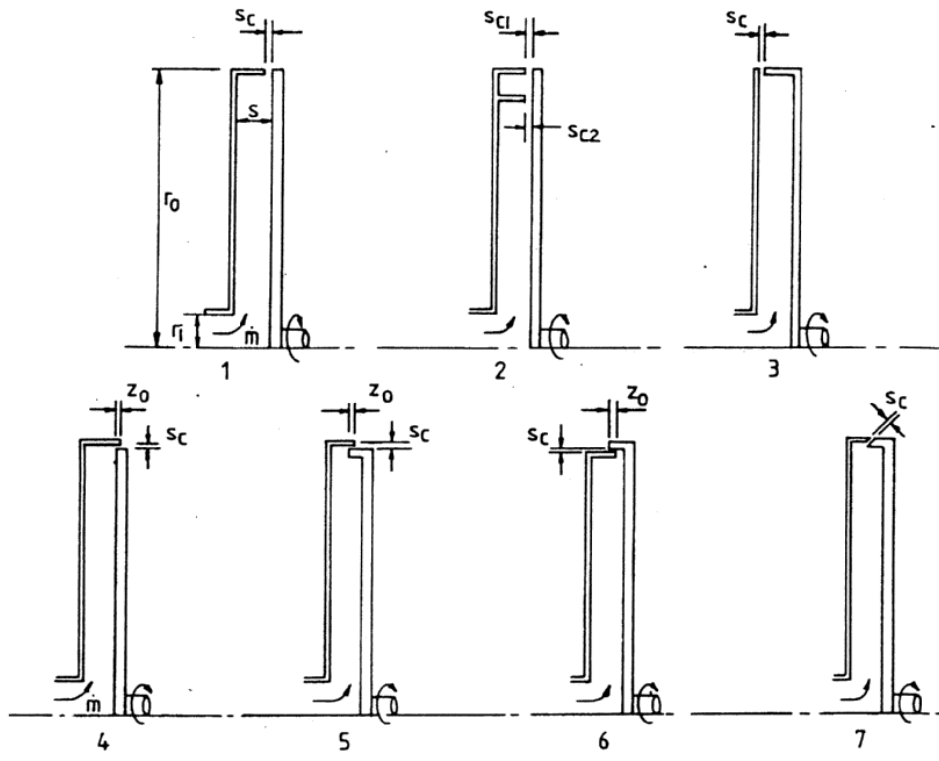
Figure 4-2   **Experimental Configuration run by Owen & Phadke to determine seal effectiveness.**
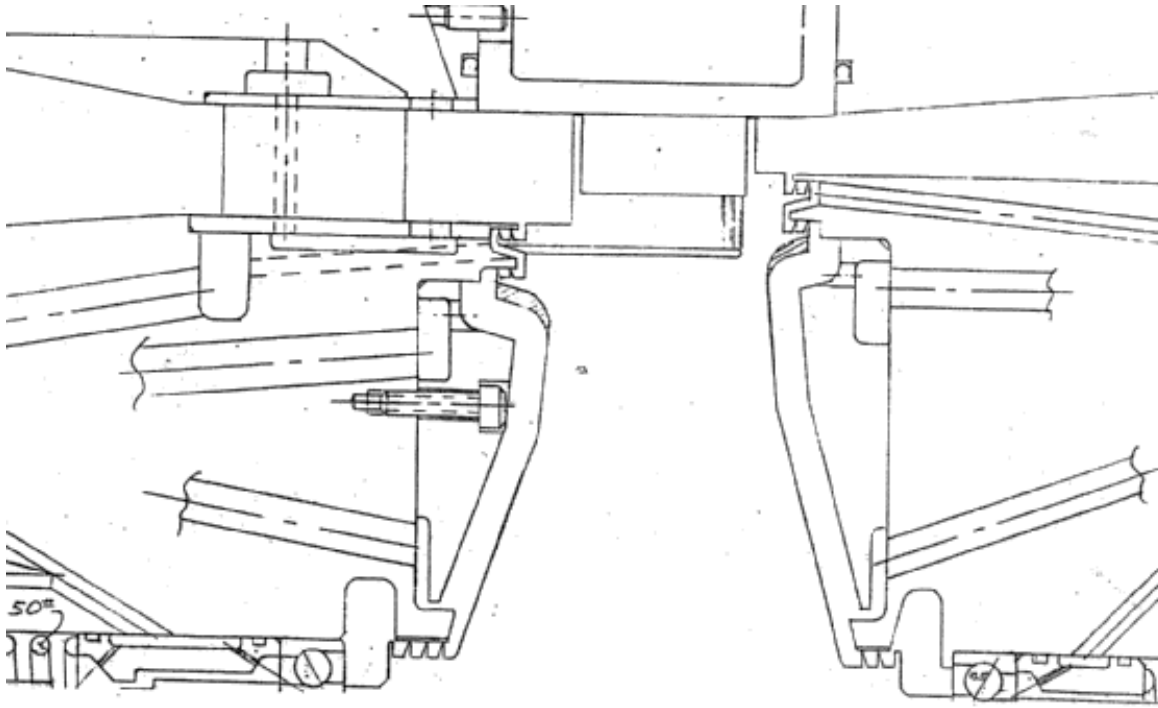
RPM	Forward Wheel Space			Aft Wheel Space		
	P (psia)	T (F)	Mass flow rate (lbm/s)	P (psia)	T (F)	Mass flow rate (lbm/s)
105000	112	235	0.048	60	239	0.027
49037	95	272	0.055	20	280	0.017
40507	121	275	0.105	20	280	0.024

Figure 4-3   Secondary buffer flows in the wheel space cavities.

$A_{exhaust}$ (360°)

Ai

Direction of flow

Ae

A_{intake} (360°)
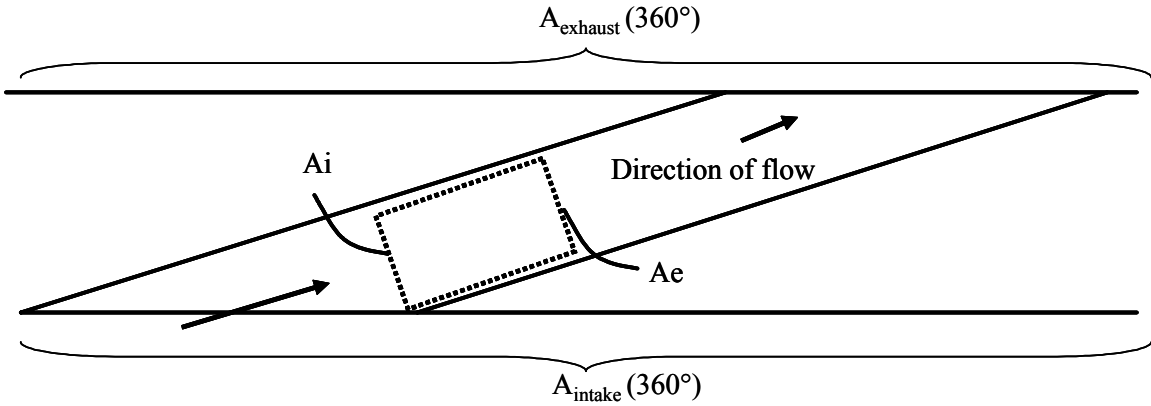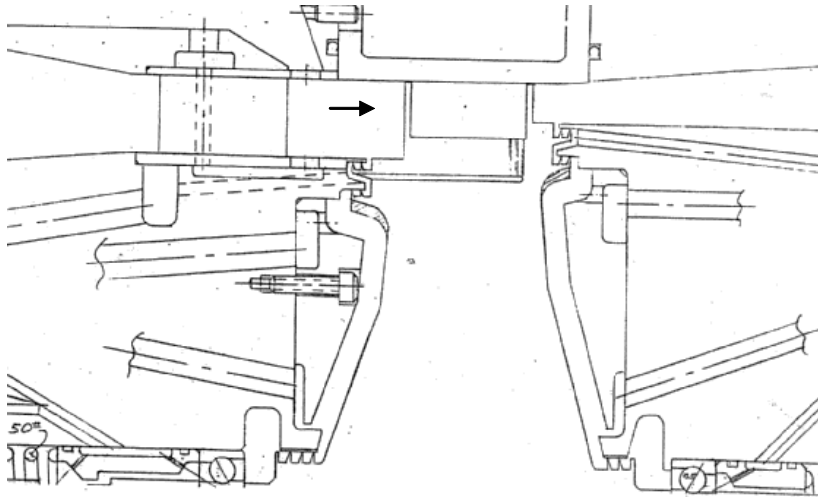
Note: Above is the top view of the Ramgen rotor flow path

Figure 4-4   **Depiction of cross-sectional areas used for axial thrust calculations.**

Un-Started Inlet With No Back Pressure

Fast

Started Inlet With No Back Pressure

Slow

Started Inlet With Maximum Back Pressure

Fast

Un-Started Inlet With Maximum Back Pressure
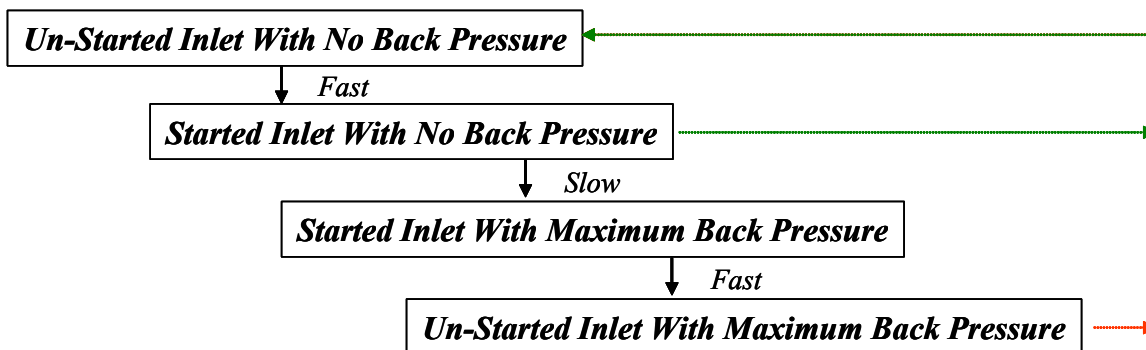
Figure 4-5   **Typical sequence of events in a Supersonic Inlet Operation**
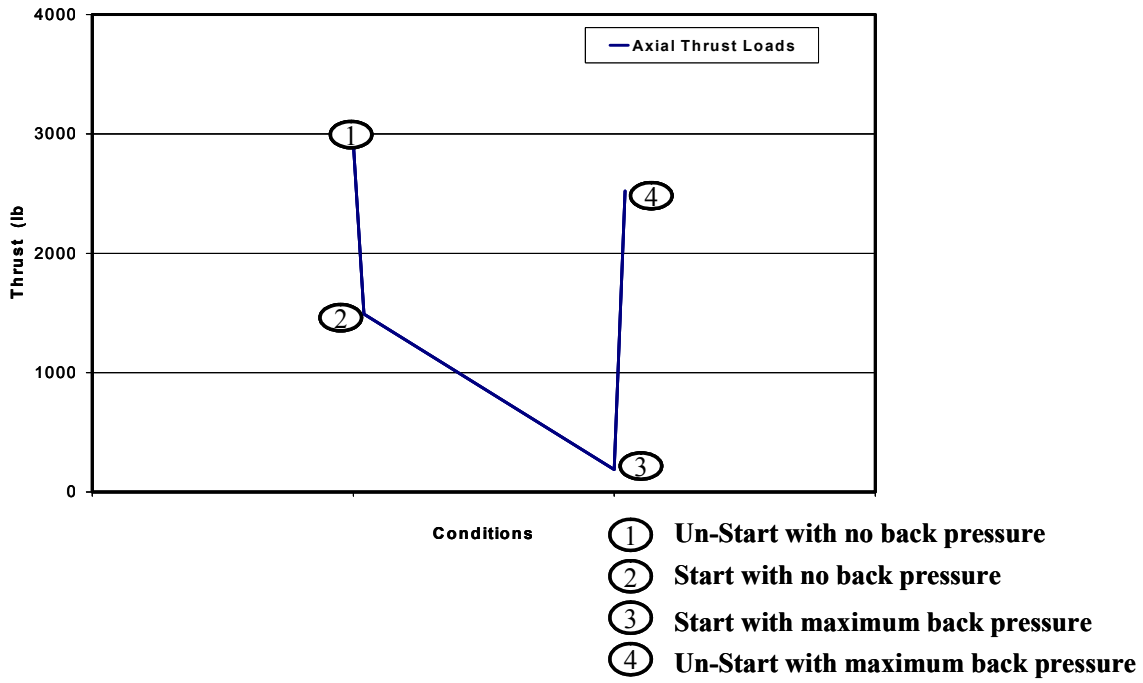
Figure 4-6   **Typical axial thrust experienced by the rotor with an active control of the wheel space cavity pressures.**

The legend for the chart conditions:
1. Un-Start with no back pressure
2. Start with no back pressure
3. Start with maximum back pressure
4. Un-Start with maximum back pressure
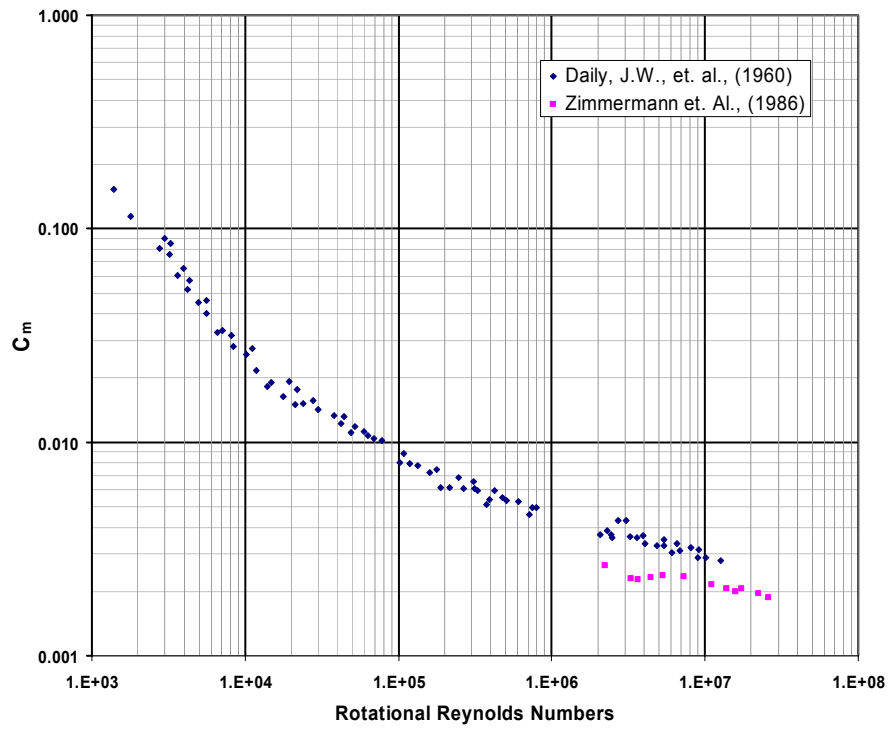
Figure 4-7 **Experimental data for dimensionless disk drag coefficient versus Rotational Reynolds Number.**
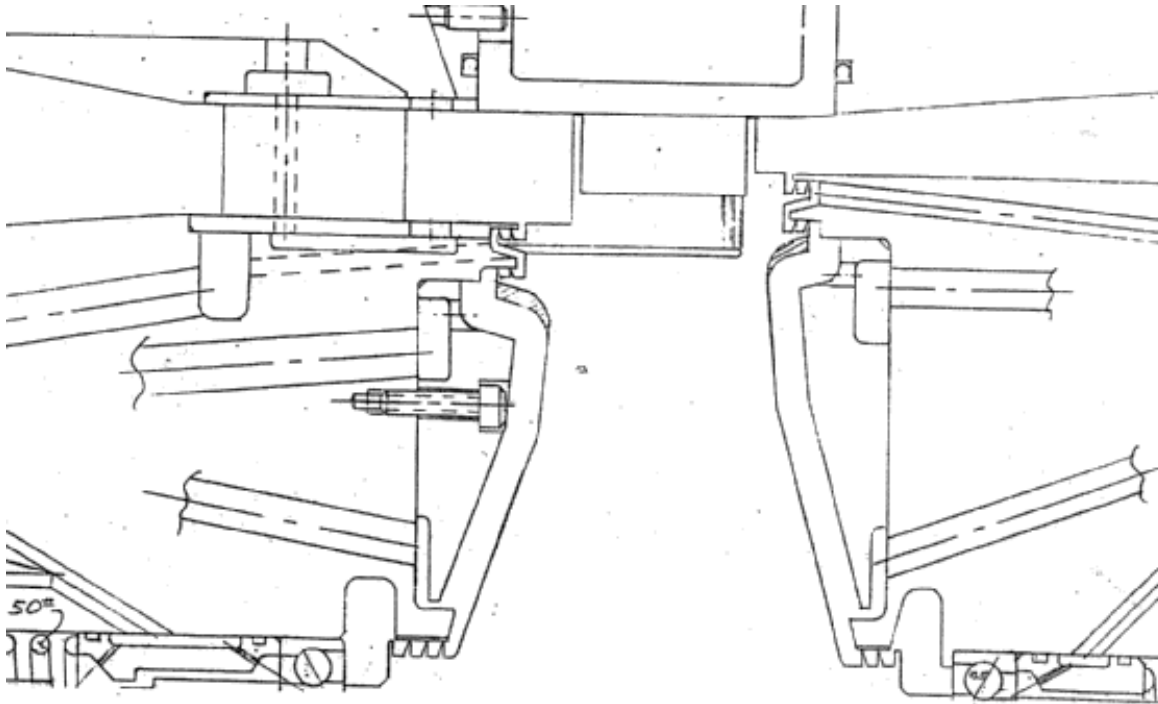
RPM	Forward Cavity Seals		Aft Cavity Seals	
	Forward Outer Rim Seal mdot (lbm/s)	Forward Hub Seal mdot (lbm/s)	Aft Outer Rim Seal mdot (lbm/s)	Aft Hub Seal mdot (lbm/s)
105000	0.019	0.012	0.104	0.004
49037	0.029	0.018	0.111	0.004
40507	0.042	0.023	0.147	0.004

Figure 4-8   Estimated Leakage flows across the Seals.

RPM	Wheel Space Drag (Hp)		
	Forward Cavity	Aft Cavity	Total
105000	32	5	37
49037	16	7	23
40507	22	10	31

Table 4-1   Estimated Drag at different rotor design speeds

Description	Area	Fx (lbf/ft) from BLC code	Final viscous drag (lbf)
inlet floor	1	11.23	0.683
inlet strake wall	5	11.23	0.680
ramp	2	3.22	0.372
ramp strake walls	6,9	3.05	0.259
expansion floor	3	2.41	0.278
expansion strake walls	7,10	2.41	0.141
exit floor	4	6.46	0.393
exit strake wall	11	6.46	0.220
		ONE FLOWPATH TOTAL DRAG==>	3.026

Table 4-2   Viscous Drag Results for One Flowpath on the Rotor.
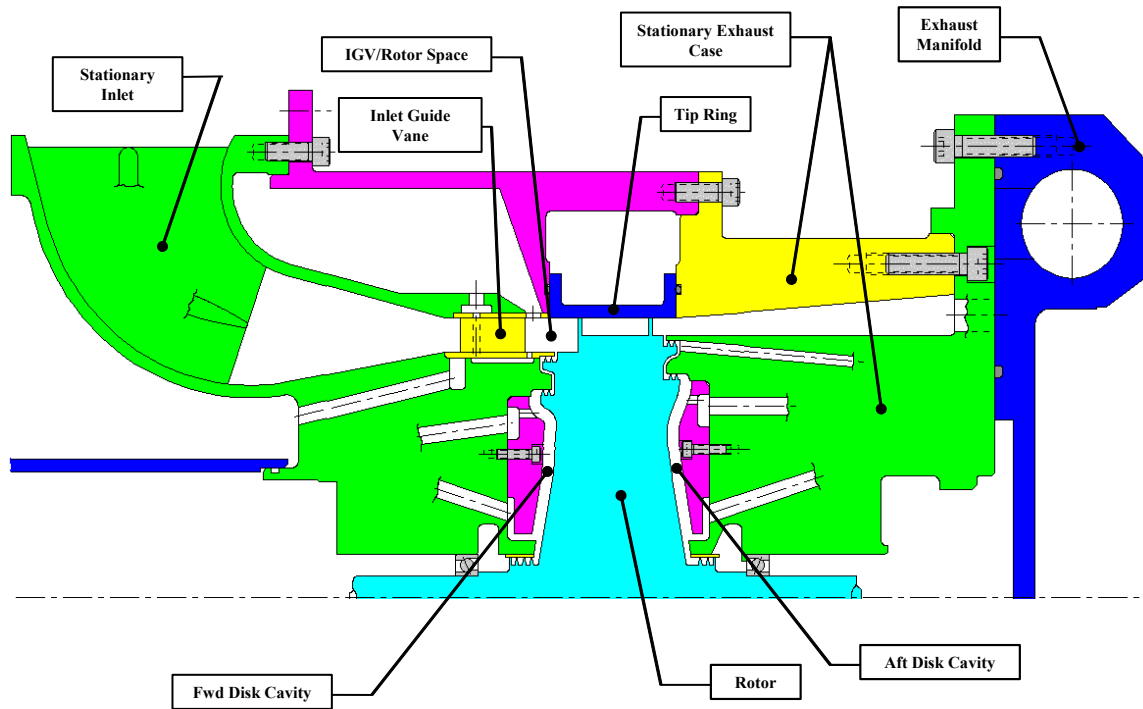
Figure 4-9 **Cross Section Illustrating The Various Rig Components**
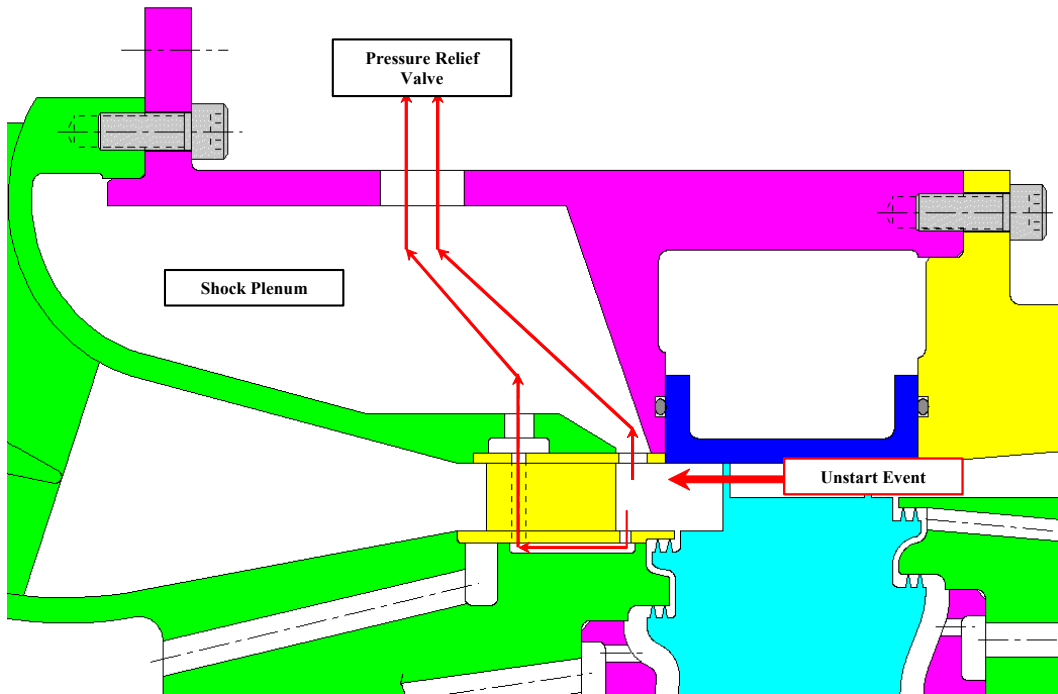
Figure 4-10   Detailed Cross Section Of The Air Inlet

Forward Disk Cavity

Outboard Seal

Seal Buffer Flow

Ingress from Main Flow

Inboard Seal

Disk Bleed (Vacuum) Flow

Cavity Out-Flow

Thrust Piston Area (Axisymmetric)

Forward Cavity Buffer/Thrust Balance In-Flow

Bearing Buffer Flow
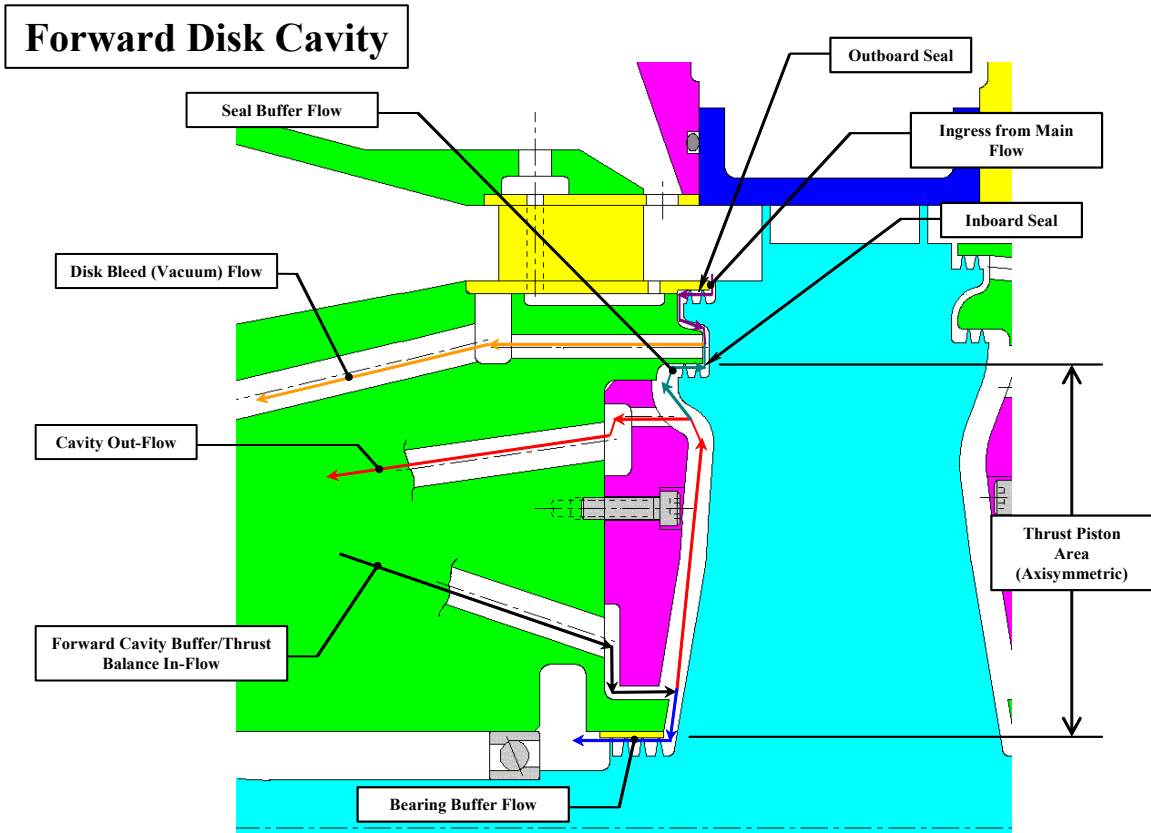
Figure 4-11   Illustration of the Forward Disk Cavity

Aft Disk Cavity

Ingress from Main Flow

Seal Buffer Flow

Outboard Seal

Inboard Seal

Seal Out-Flow

Cavity Out-Flow

Aft Cavity Buffer In-Flow

Cavity Purge Flow

Bearing Buffer Flow
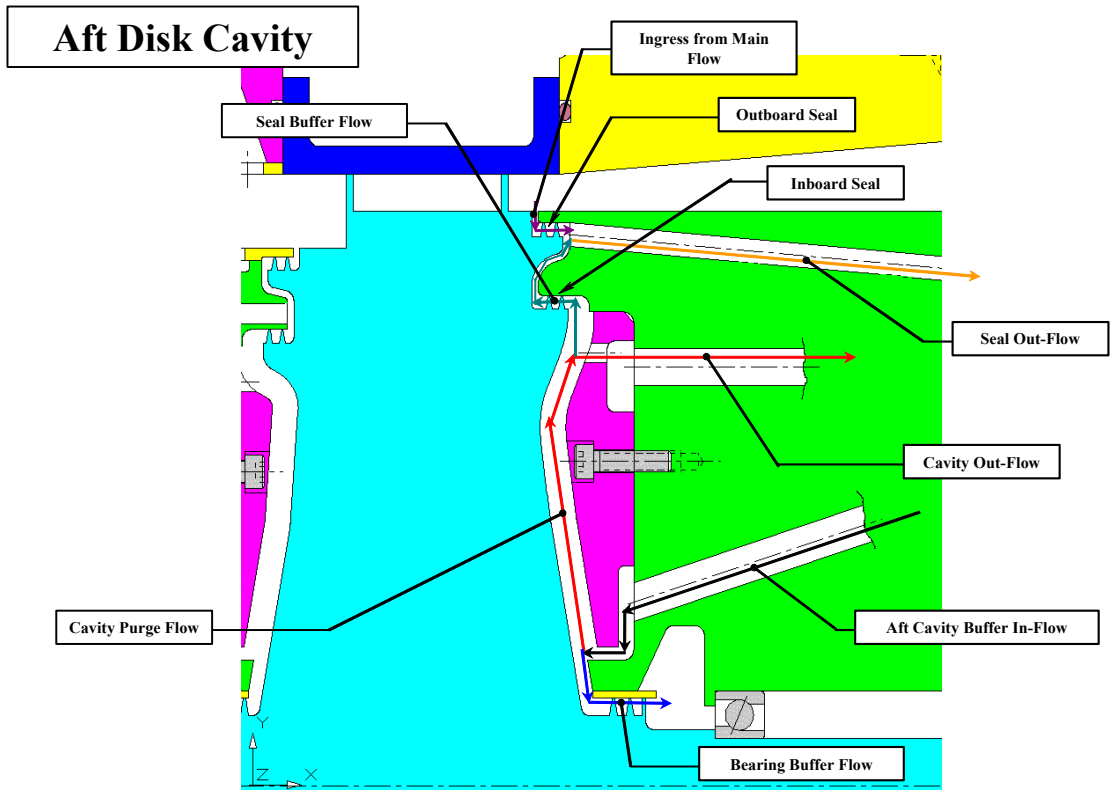
Figure 4-12   Illustration of the Aft Disk Cavity

$F_3 = P_3 \times A_3$

$F_1 = P_1 \times A_1$

$F_2 = P_2 \times A_2$

$P_1 =$ Forward Disk Cavity Buffer Flow Pressure

$P_2 =$ Aft Disk Cavity Buffer Flow Pressure

$P_1 =$ Rotating Inlet Exhaust Pressure
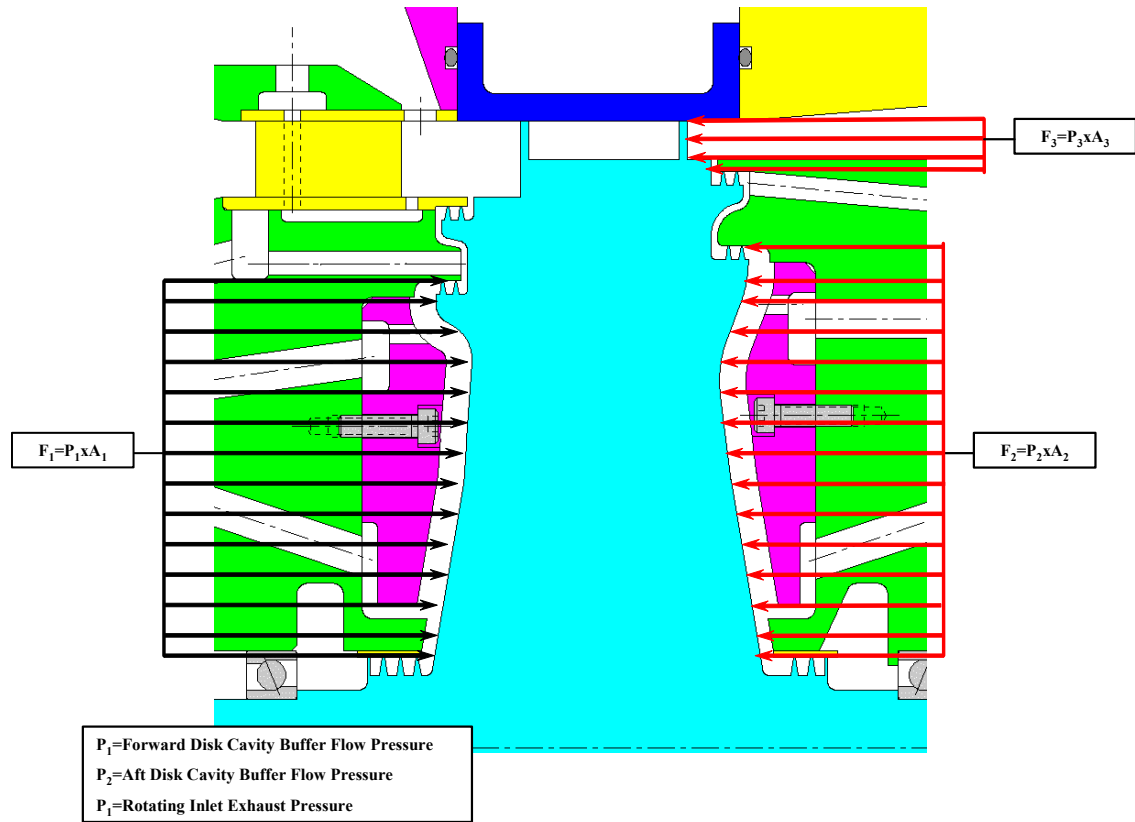
Figure 4-13   Illustration of the Thrust Balance System
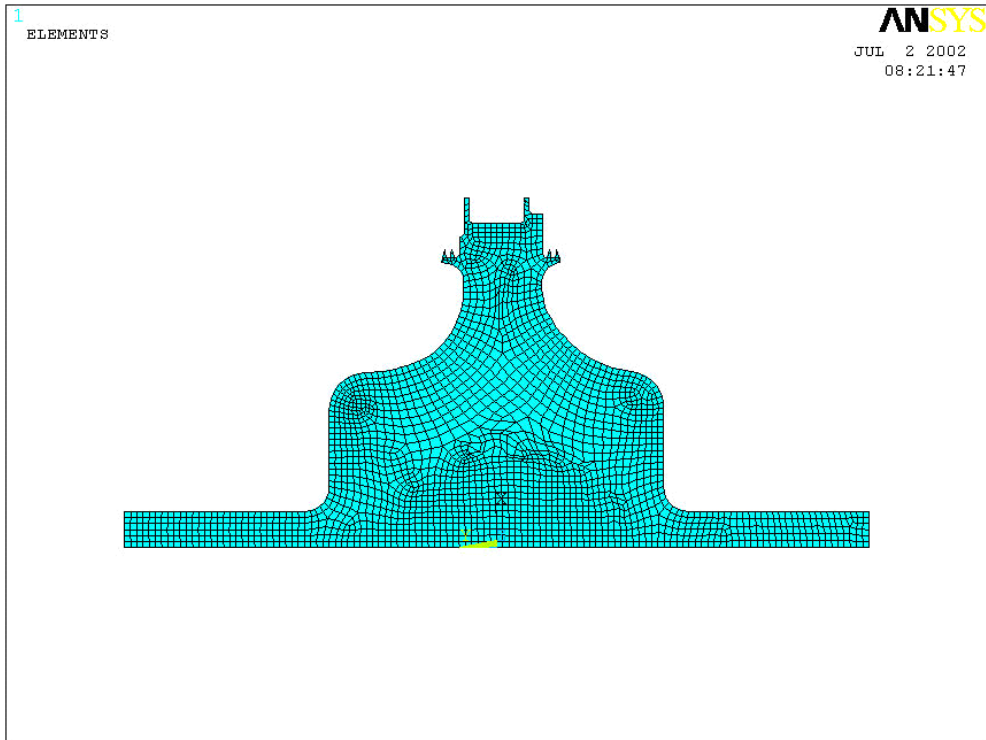
Figure 4-14   2D Axisymmetric Model Of The Compressor Rotor.
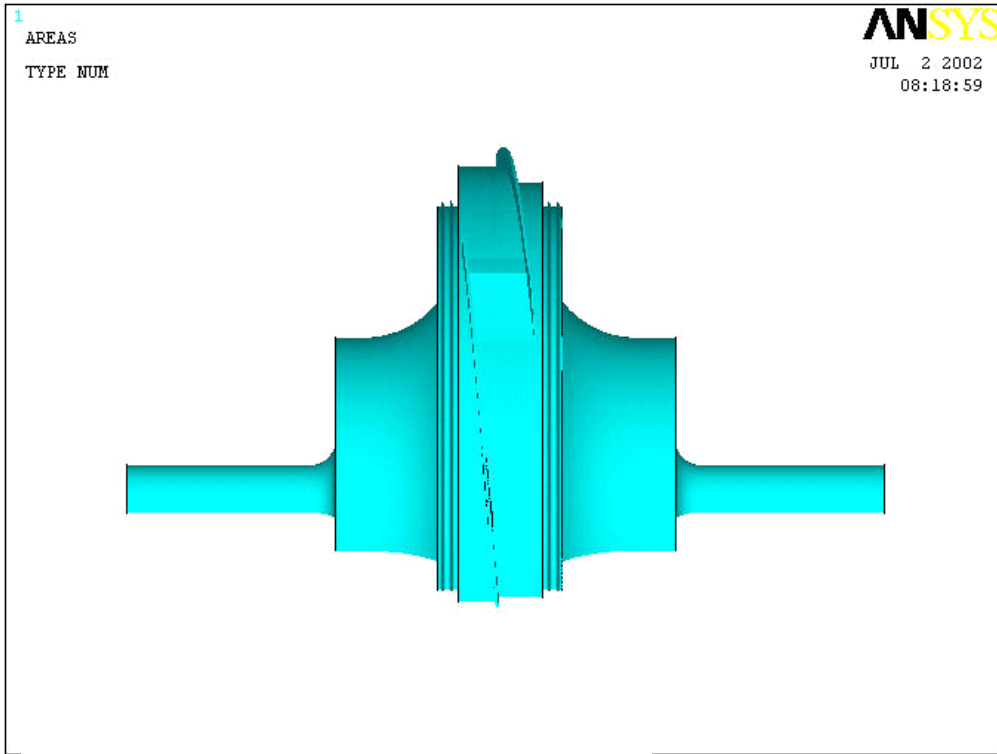
Figure 4-15   3D 120° Sector Model Of The Compressor Rotor.
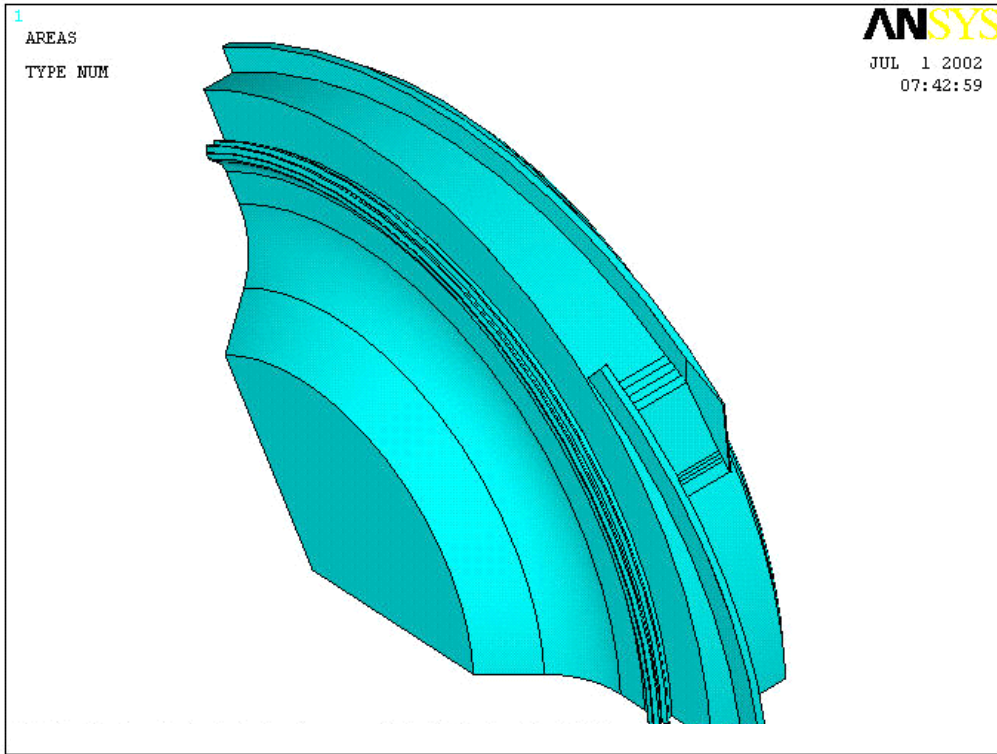
Figure 4-16   3D 120° Sector Model Of The Compressor Rotor.
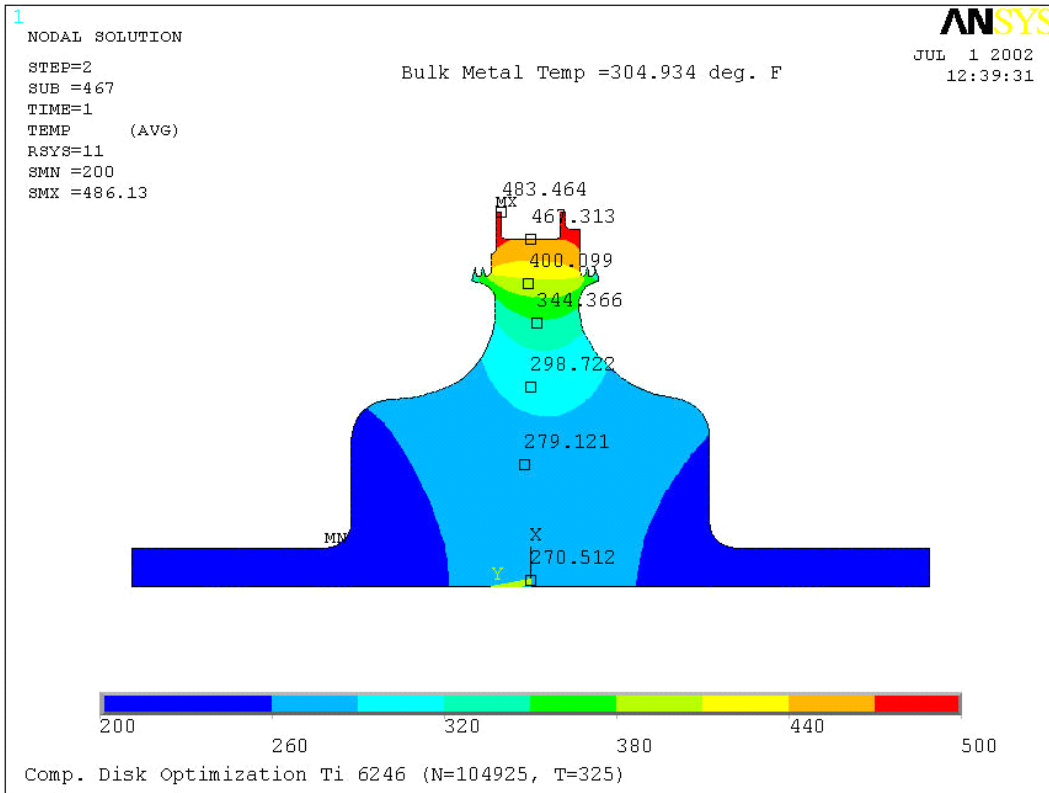
Figure 4-17   2D Full Load Steady State Temperature Profile Of the Rotor.
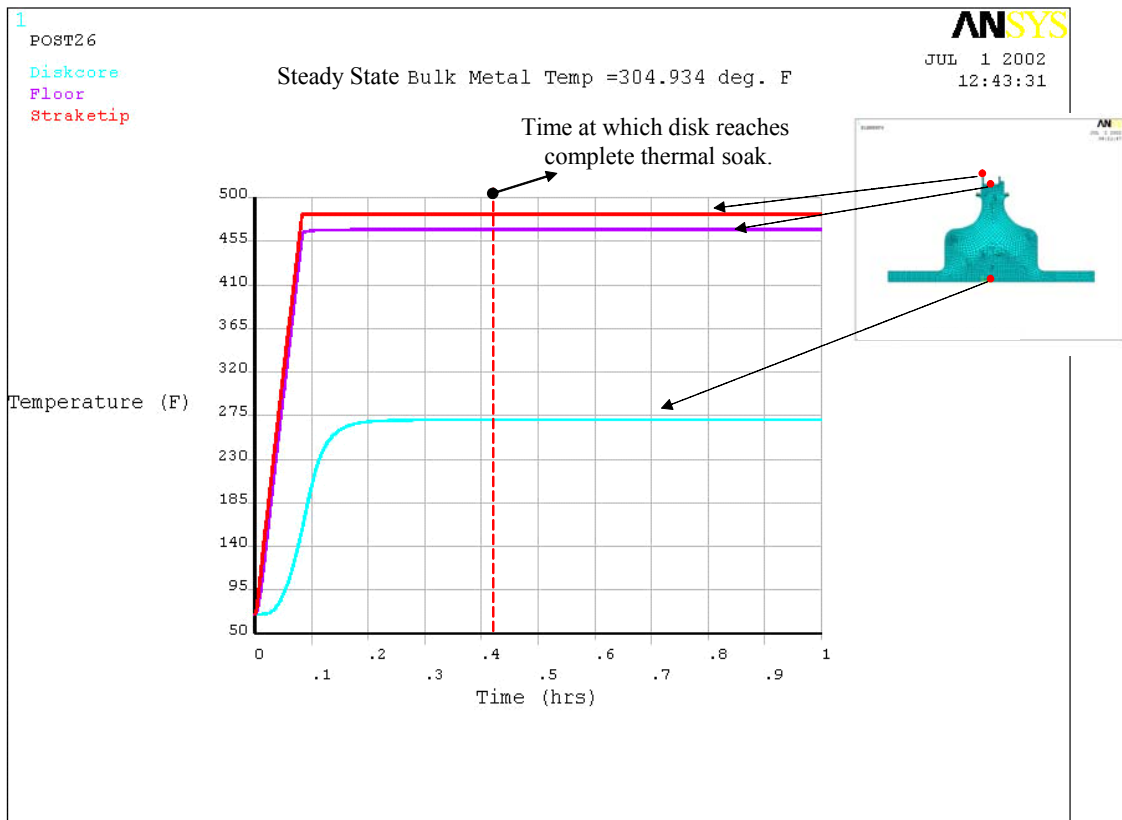
Figure 4-18   2D Transient Temperature Profile Of the Rotor.
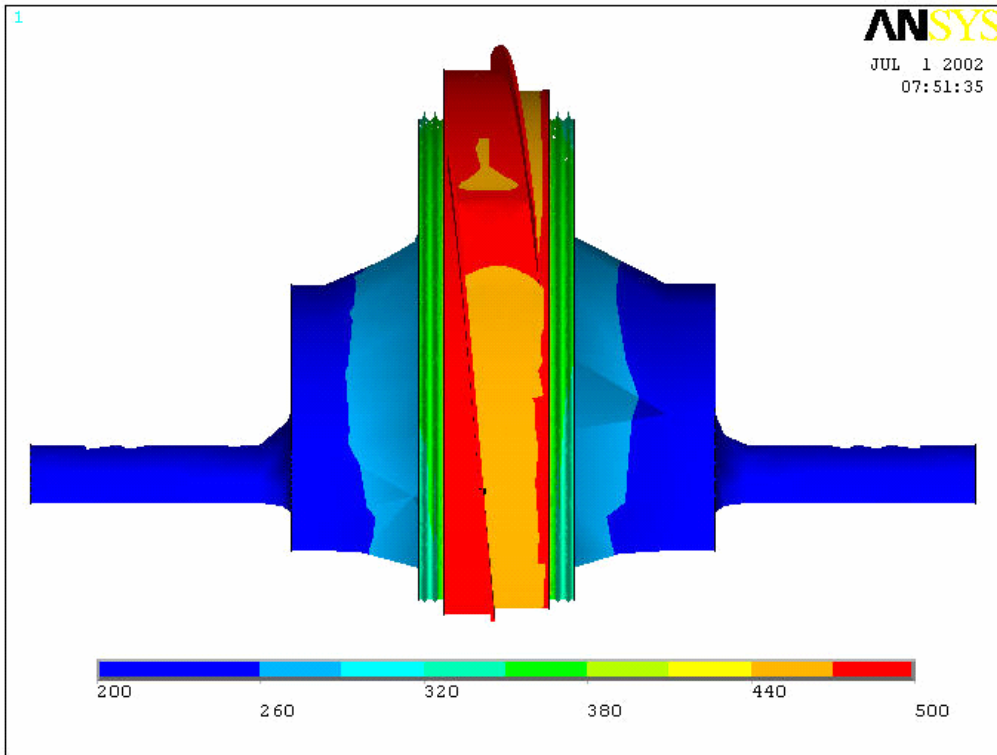
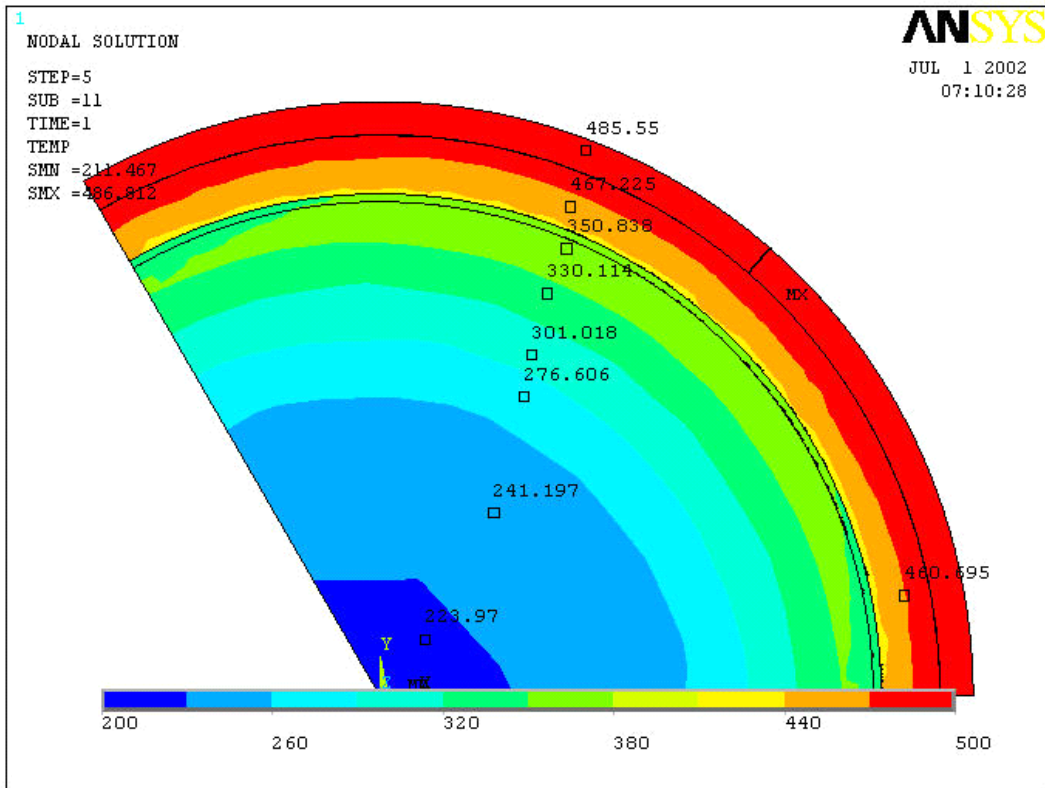**Figure 4-19   3D Full Load Steady State Temperature Profile Of the Rotor.**
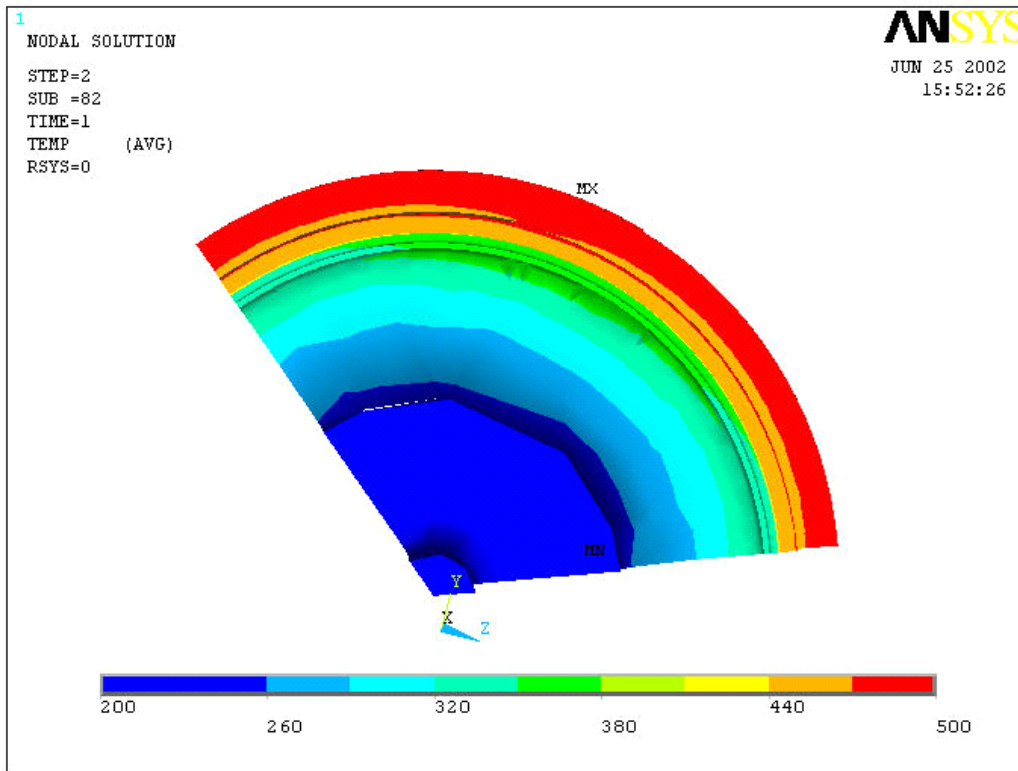
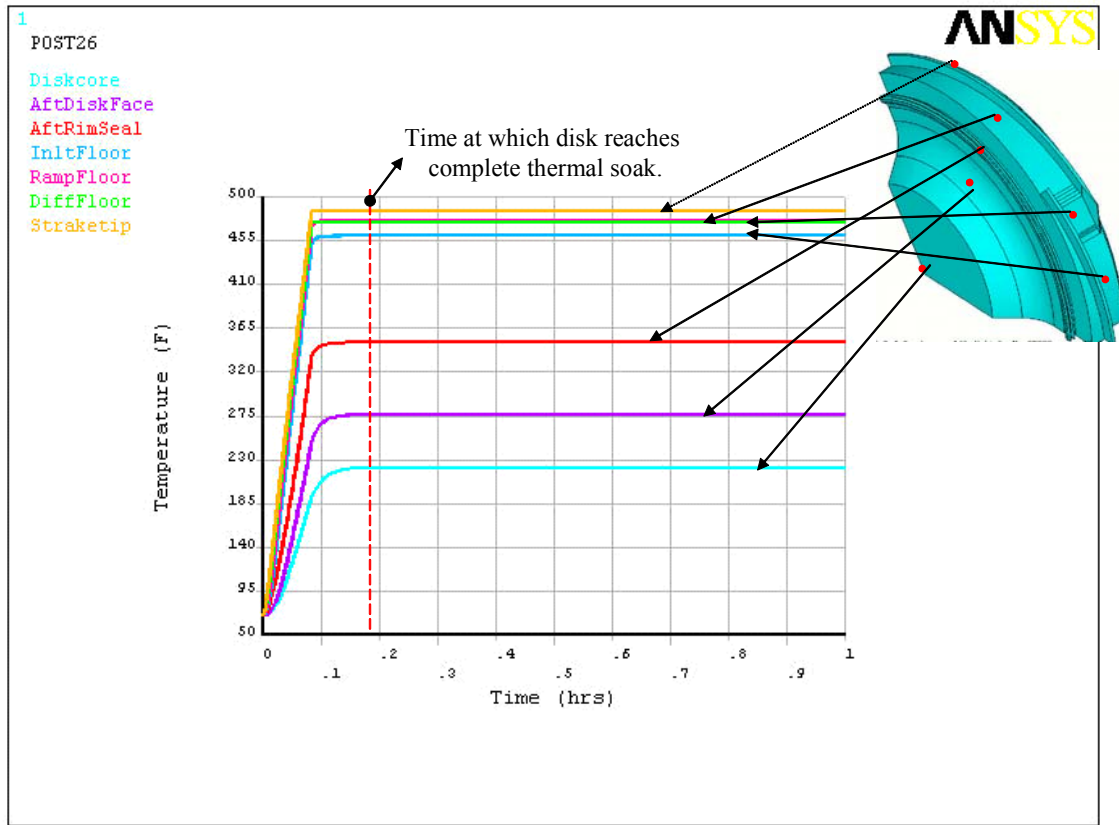**Figure 4-20　　3D Full Load Steady State Temperature Profile Of the Rotor.**
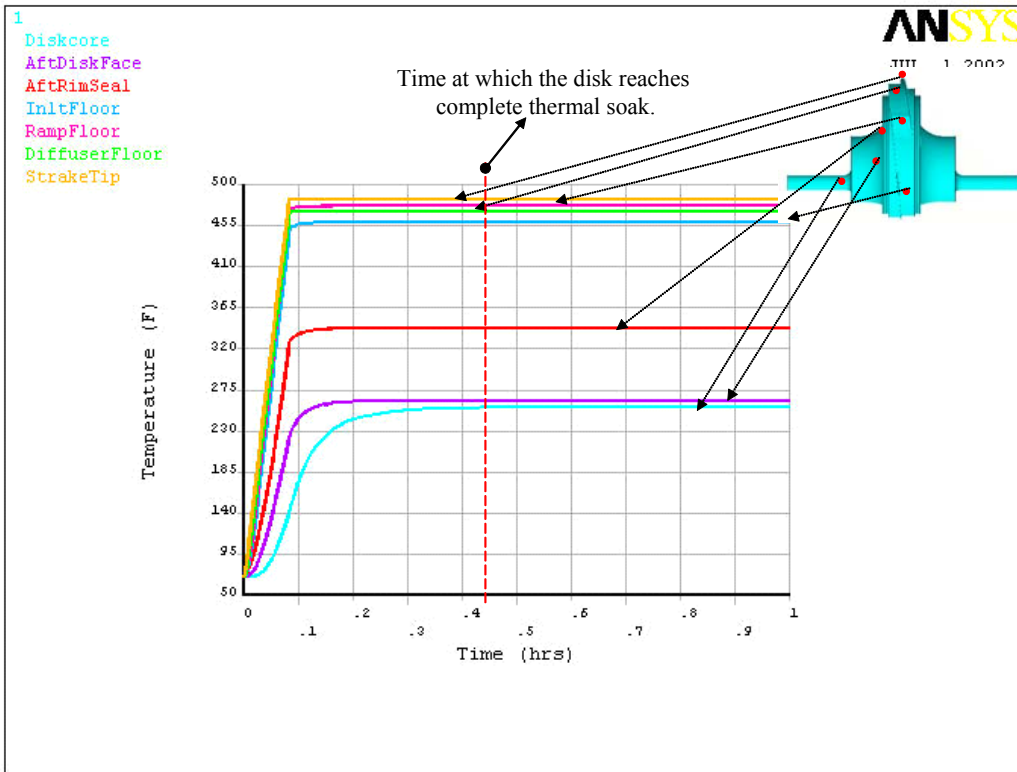
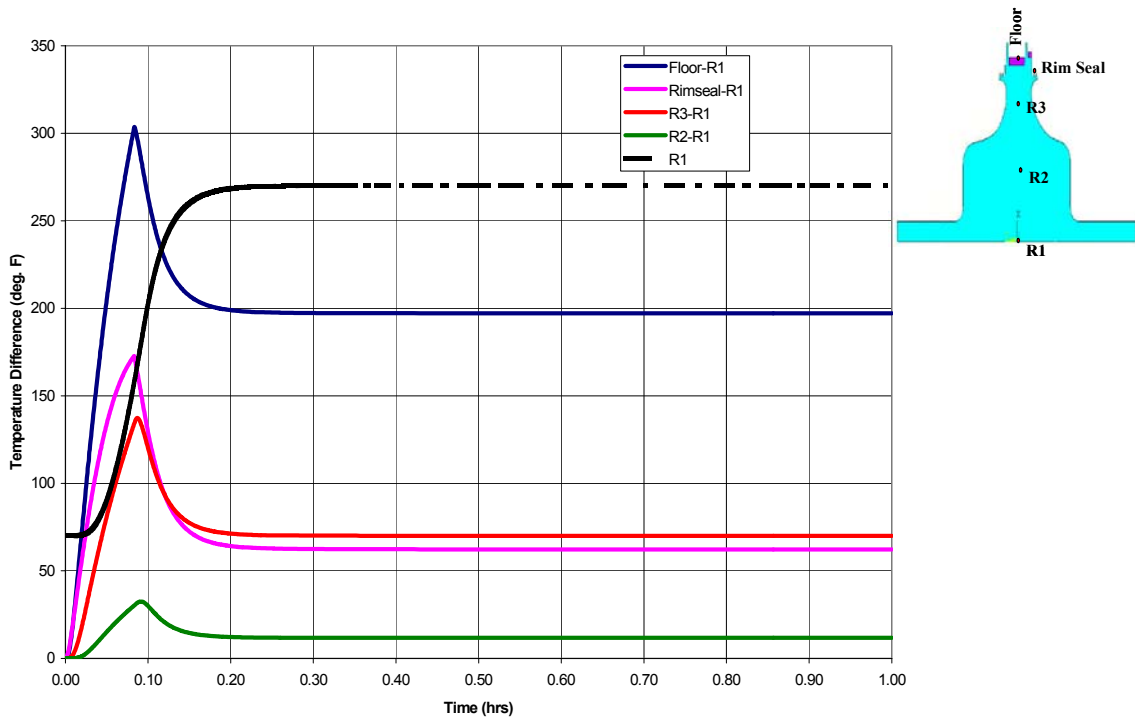**Figure 4-21   3D Transient Temperature Profile Of the Rotor.**
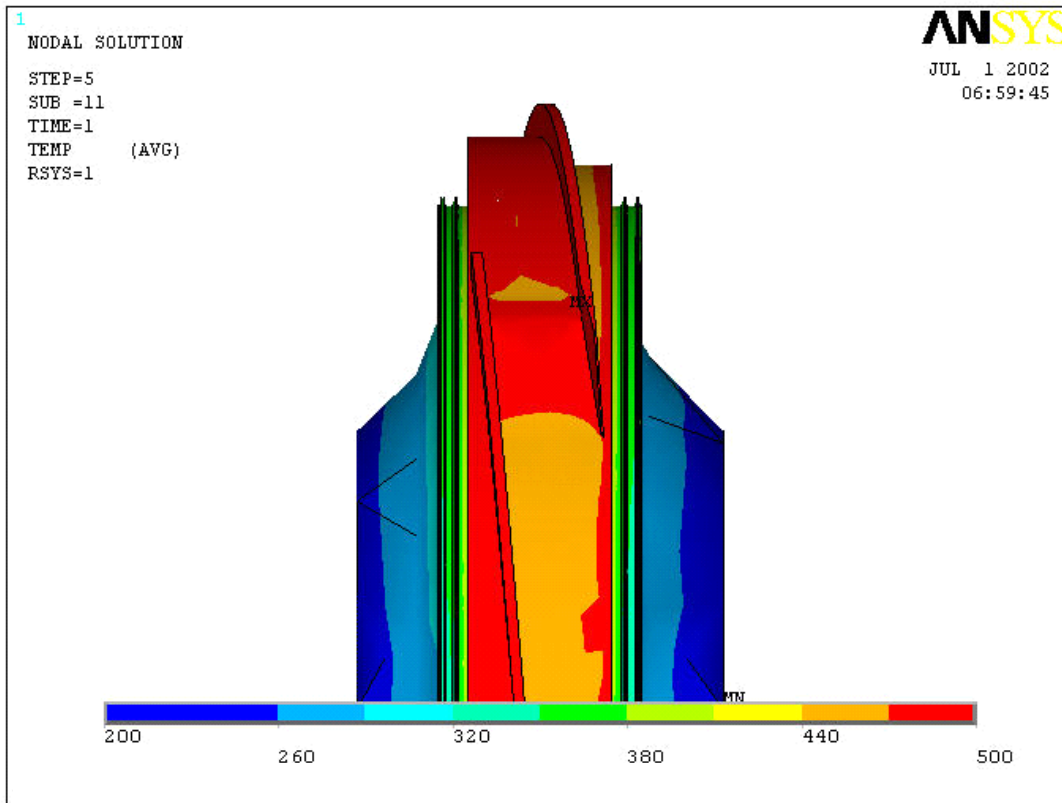
Figure 4-22 **3D Full Load Steady State Temperature Profile Of the Rotor.**

Figure 4-23   3D Full Load Steady State Temperature Profile Of the Rotor.

Figure 4-24   3D Transient Temperature Profile Of the Rotor.

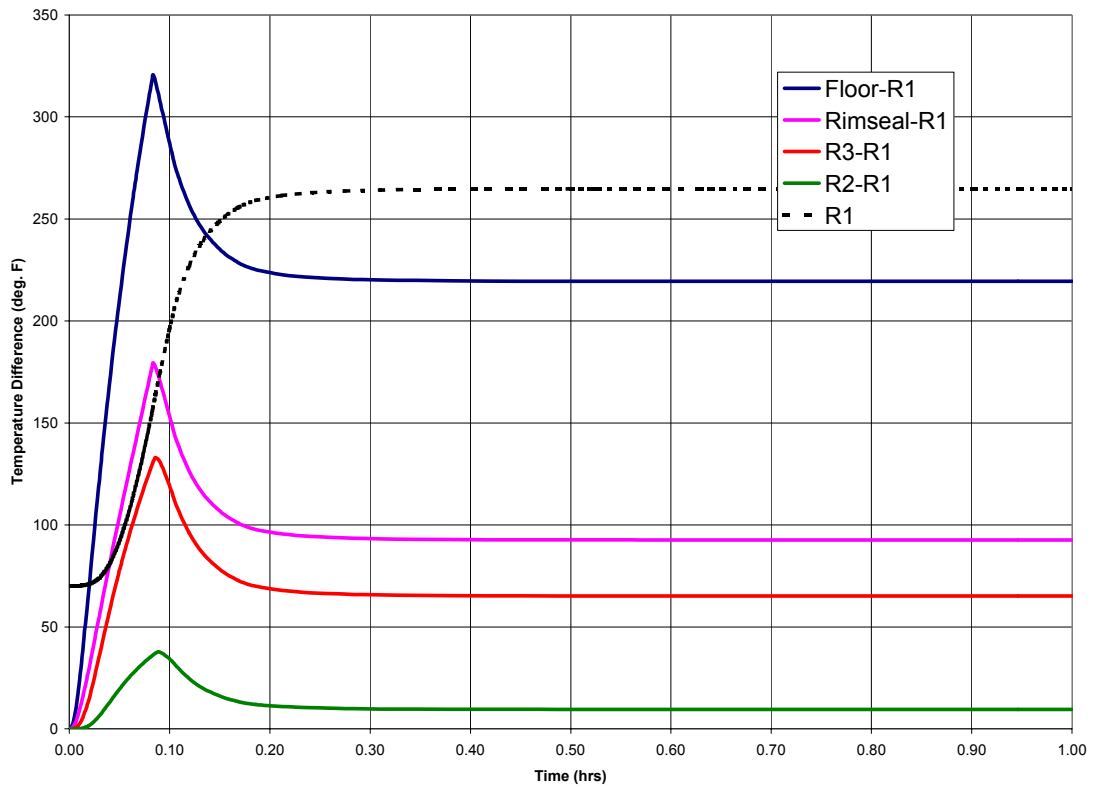**Figure 4-25   2D Transient Temperature Difference Profile Of the Rotor.**

Figure 4-26   3D Transient Temperature Difference Profile Of the Rotor (For Rotor shape in Figure 4-15).
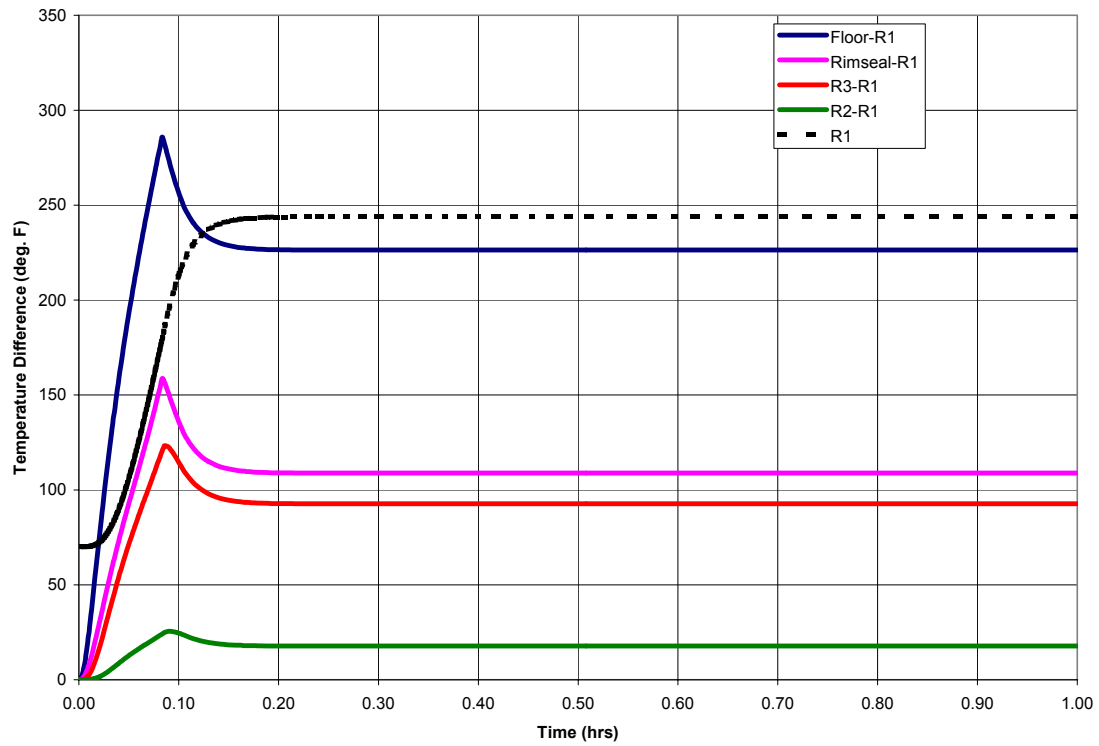
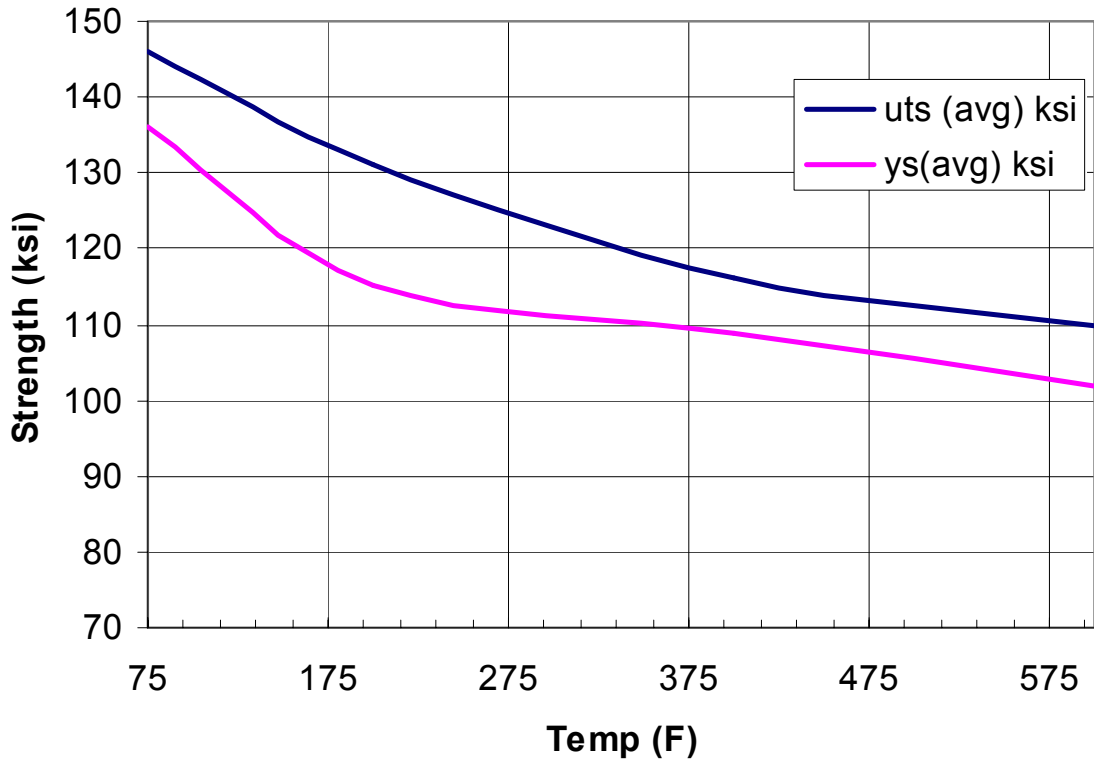**Figure 4-27** **3D Transient Temperature Difference Profile Of the Rotor (For Rotor shape in Figure 4-16).**

Figure 4-28   **Variation of Ti 6242 mechanical strength properties with temperature.**
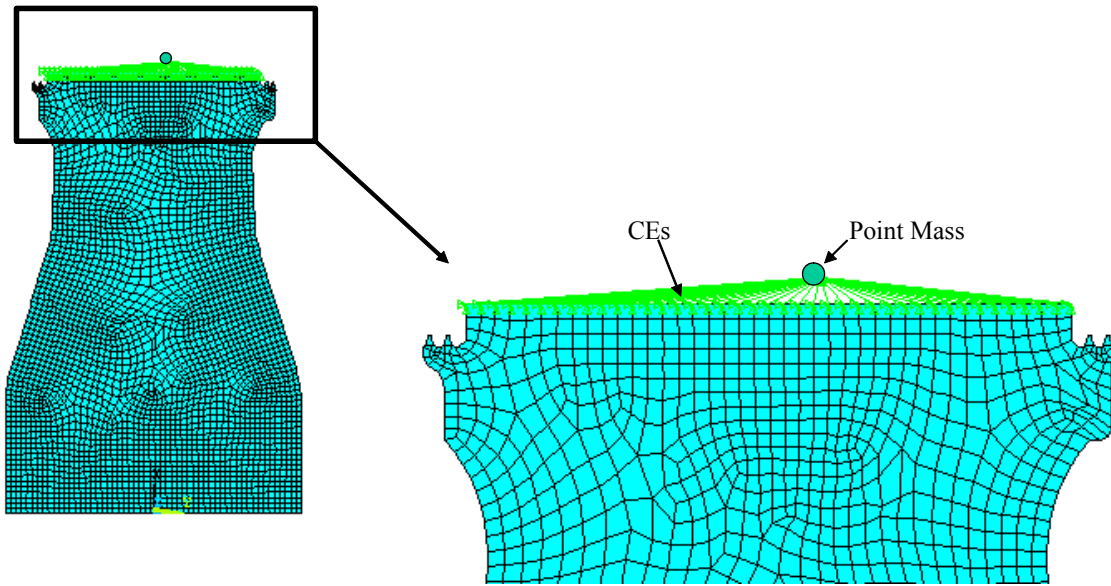
Figure 4-29   2D Disk modeling approach for optimization.
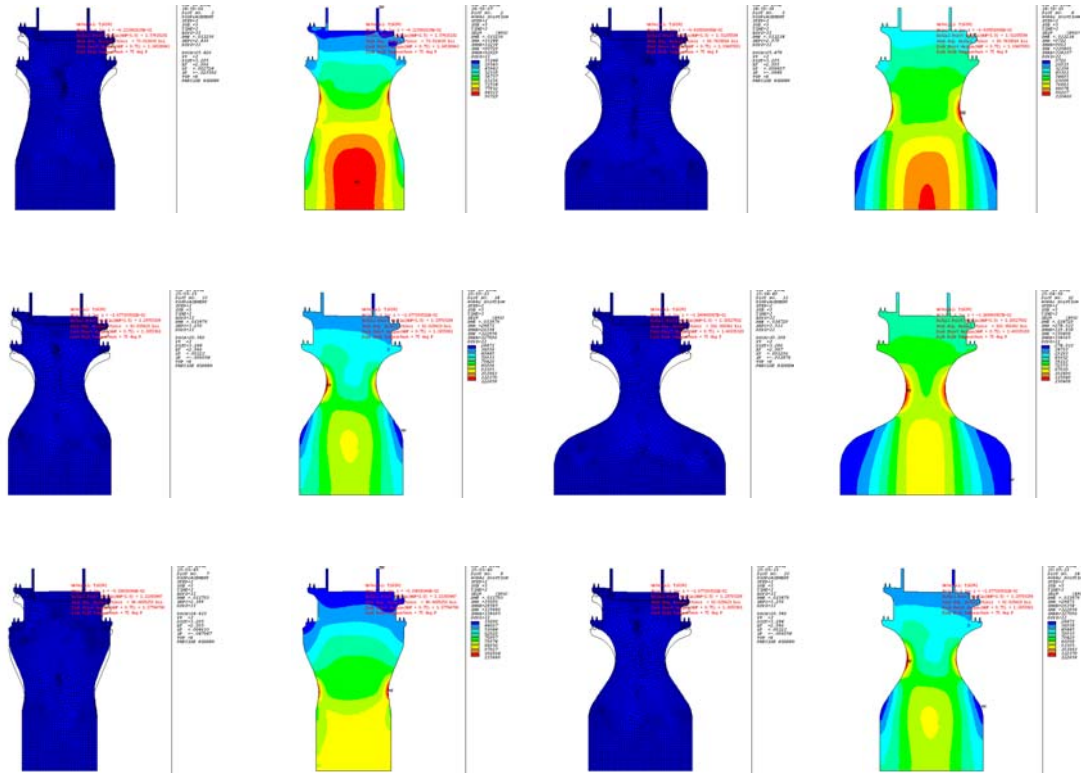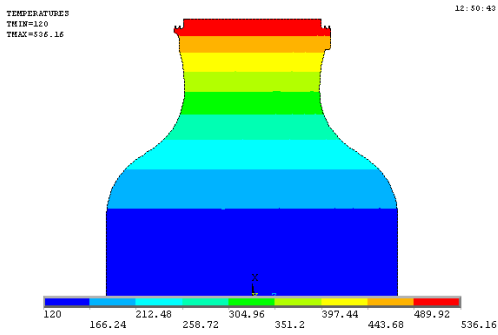
Figure 4-30   **A sampling of disk shapes and the corresponding plots of equivalent stresses generated by the optimizer for the 16:1 pressure ratio design.**

TEMPERATURES
TMIN=120
THAX=536.16

12:50:43

Disk bulk temp = 320F

Burst Margin > 125 %

Rotor Wt = 27 lb

120   212.48   304.96   397.44   489.92
   166.24   258.72   351.2   443.68   536.16

Radial Temperature distribution

3
1
(AVG)
.014229
9761
93185
11

12:49:51

Principal Stress : 93 ksi

4.2 in.

9761   28299   46838   65377   83916
   19030   37569   56108   74646   93185

3
1
(AVG)
.014229
8784
110844
11

12:50:04

Equivalent Stress :111 ksi

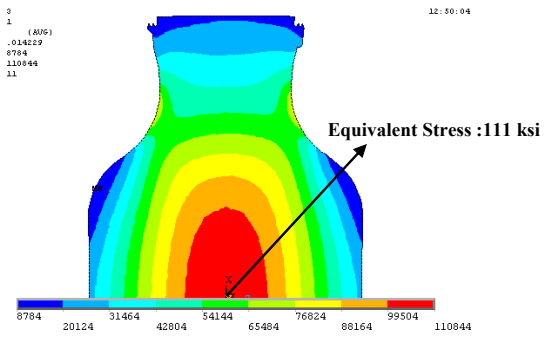8784   31464   54144   76824   99504
   20124   42804   65484   88164   110844

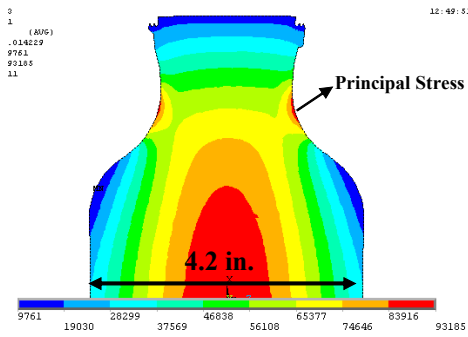**Figure 4-31   Optimized disk shapes for 54,572 rpm, 10 in disk and the corresponding plots of equivalent and principal stress.**

83.8 ksi for 40,507 rpm

48.77 ksi for 30,900 rpm

Principal Stress

A=175.394   C=226.185   E=276.972   G=327.76   I=378.549
    B=200.789   D=251.577   F=302.366   H=353.154

A=5570   C=23975   E=42381   G=60786   I=79192
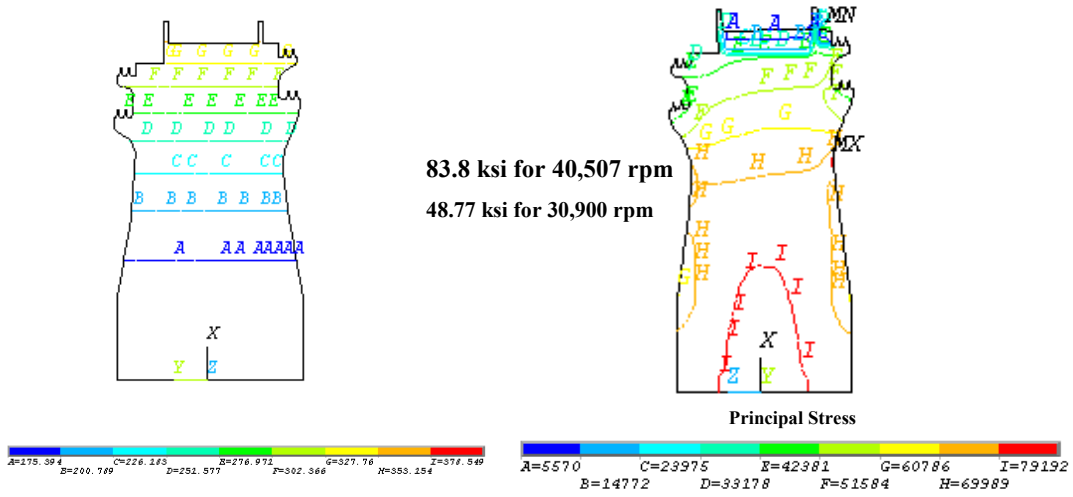   B=14772   D=33178   F=51584   H=69989

Figure 4-32   Optimized disk shape for 16:1 pressure ratio disk. Temperature and Principal stress distribution at 40507 rpm.

STEP=1
SUB =3
TIME=1
SEQV   (AVG)
DMX =.011248
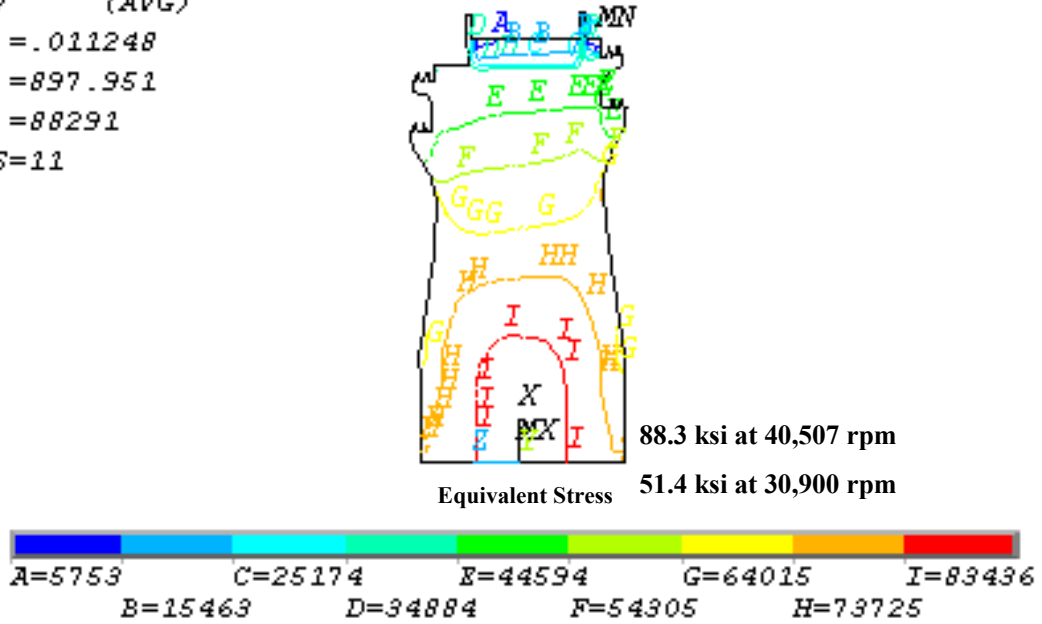SMN =897.951
SMX =88291
DSYS=11

SEP 16 200
13:43:3

88.3 ksi at 40,507 rpm

51.4 ksi at 30,900 rpm

Equivalent Stress

A=5753   C=25174   E=44594   G=64015   I=83436
     B=15463   D=34884   F=54305   H=73725

Figure 4-33   Optimized disk shape for 16:1 pressure ratio disk. Equivalent stress distribution at 40507 rpm.

CPs

Radial and axial constraint
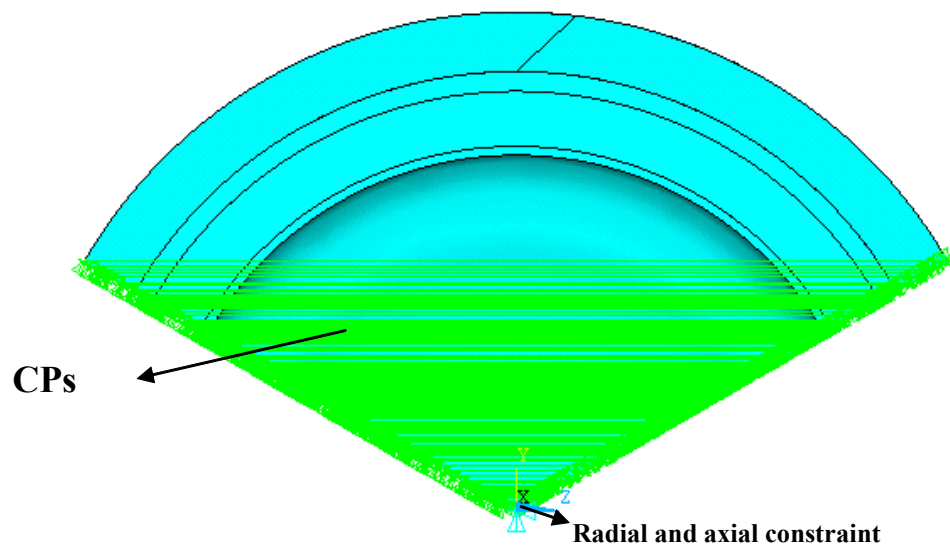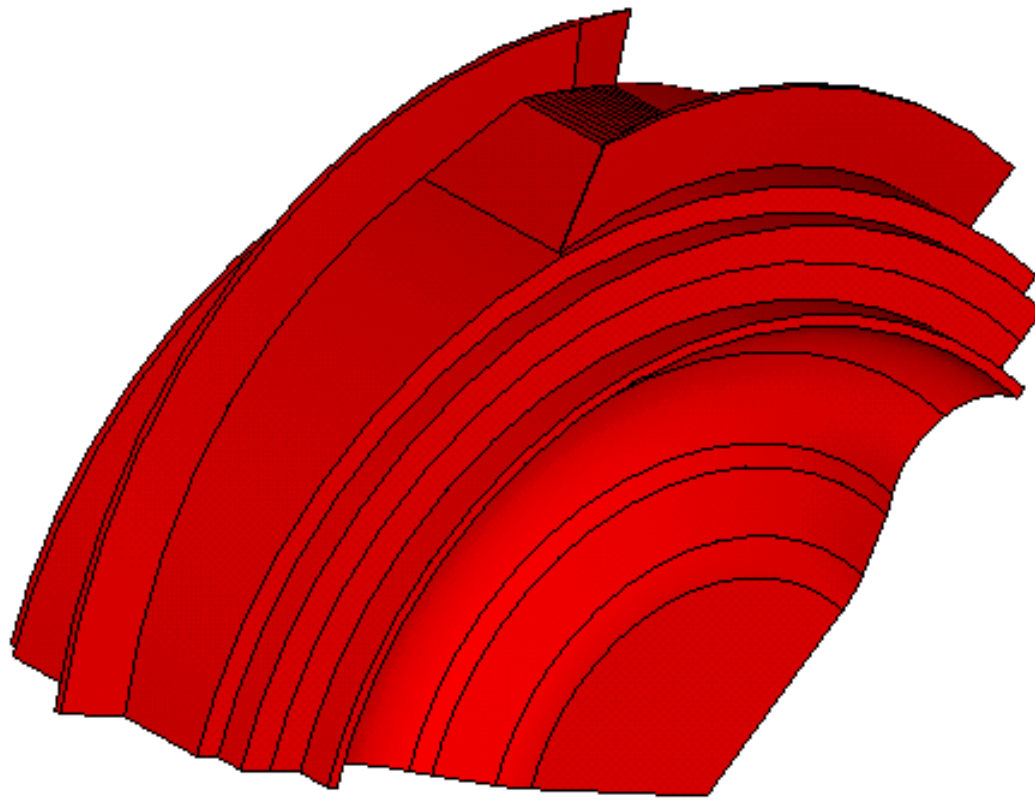
Figure 4-34 **Rotor 3D 120 degree sector model.**

85.5 ksi at 40,507 rpm

49.7 ksi at 30,900 rpm

Principal Stress

```
A=27359        C=41050      E=54741         G=68432        I=82123
      B=34204        D=47895      F=61586        H=75277
```

```
STEP=1
SUB =3
TIME=1
SEQV    (AVG)
DMX =.014037
SMN =35656
SMX =87850
DSYS=6
```

13:4

Equiv. Stress →

87.8 ksi at 40,507 rpm

51 ksi at 30,900 rpm

```
A=38556        C=50154      E=61753         G=73351        I=84950
      B=44355        D=55954      F=67552        H=79151
```
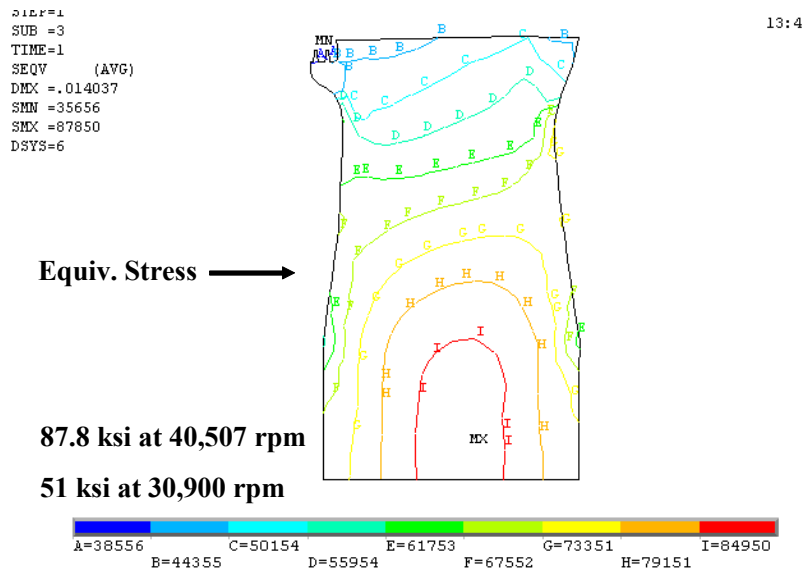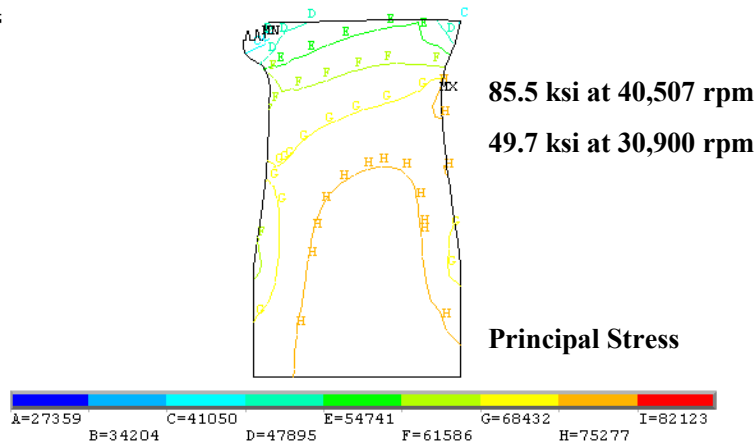
Figure 4-35   Rotor 3D 120 degree sector model stress results.
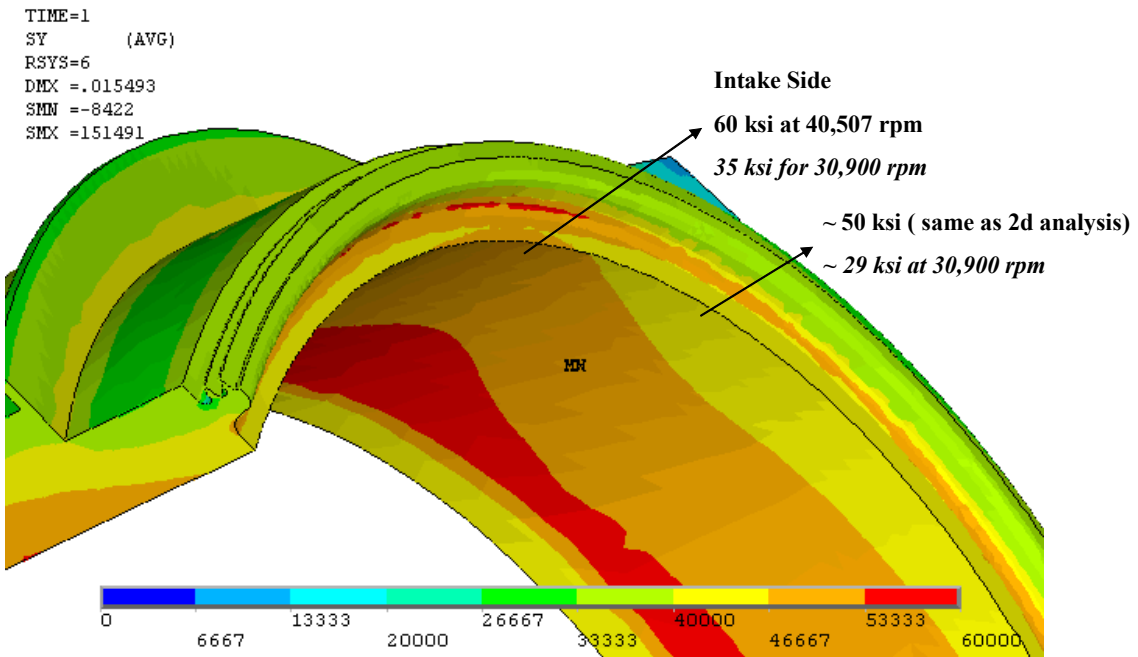
Figure 4-36 **Rotor 3D 120 degree sector model hoop stress distribution.**

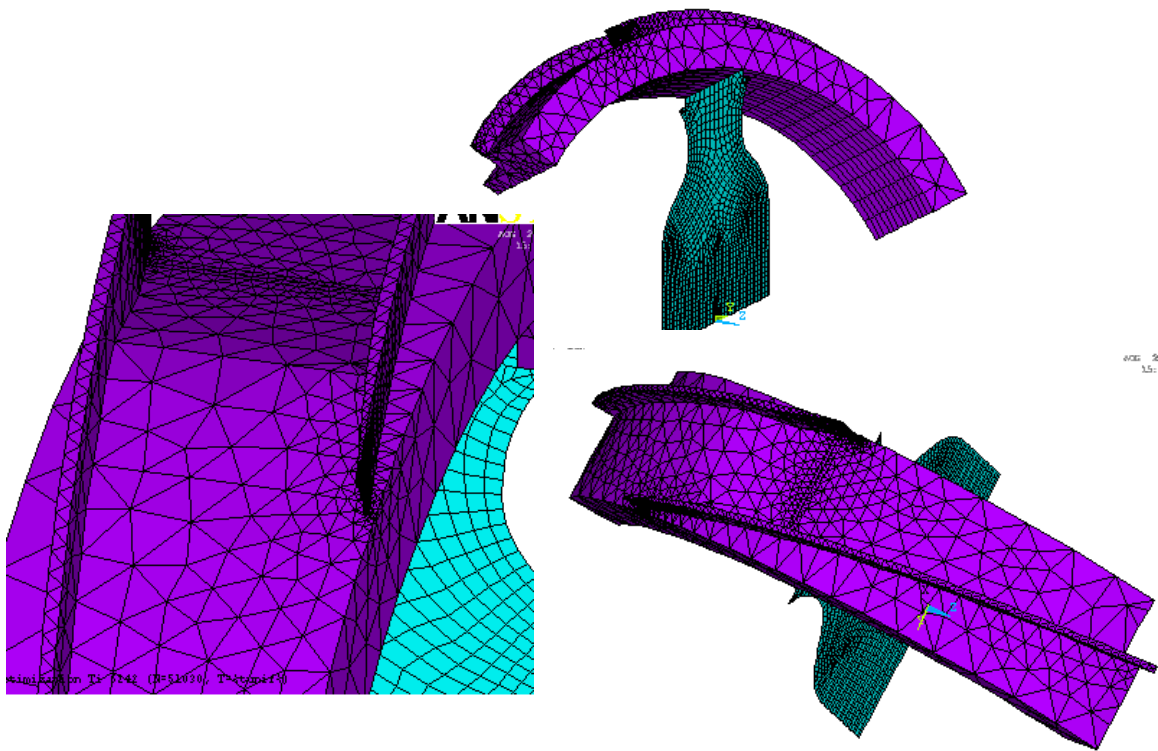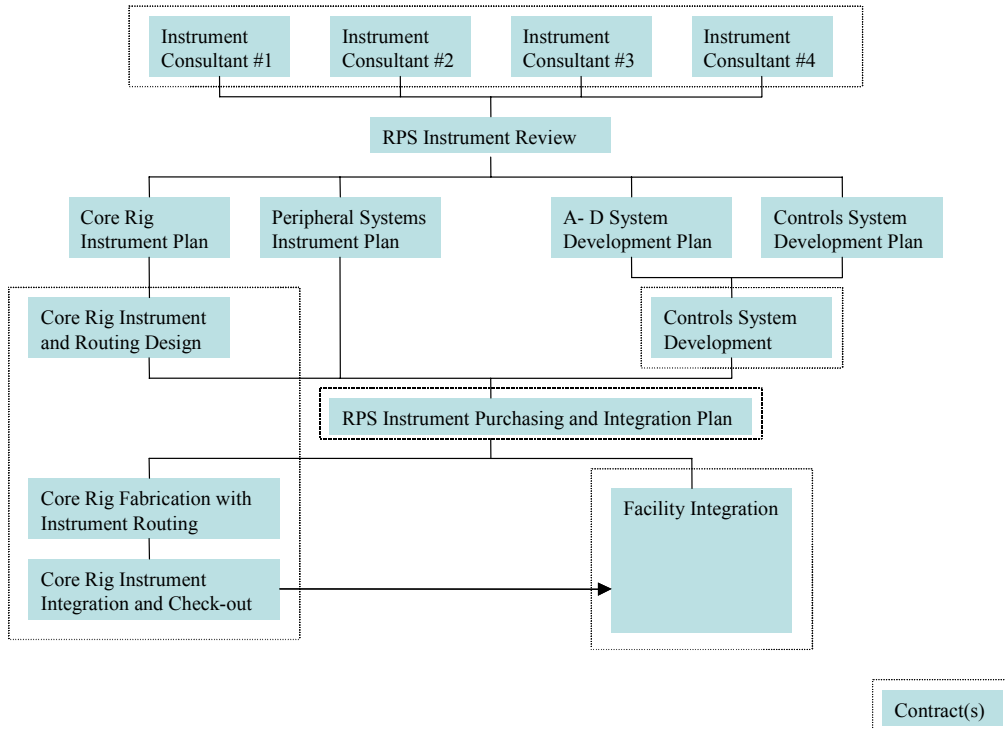**Figure 4-37** **Rotor 2D/3D model.**

Figure 4-38   Schematic Layout of Instrumentation Strategy

EXHAUST TOTAL TEMPERATURE
21, 1 MEASUREMENT AT EACH STATION
OF THE INTAKE TOTAL PRESSURE RAKES

EXHAUST STATIC PRESSURE FLUCTUATION
3 HIGH SPEED PIEZOELECTRIC PRESSURE
TRANSDUCERS, 120 DEGREES APART, 60
DEGREES FROM TOTAL PRESSURE RAKES

EXHAUST STATIC PRESSURE
12, 3 OD AND 3 ID LOCATIONS, 60 DEG SPACING, IN THE
EXIT PLANE OF THE TOTAL PRESSURE RAKE. 3 OD AND
3 ID LOCATIONS AT A TBD DOWNSTREAM LOCATION.

EXHAUST TOTAL PRESSURE
63, 3 EA. 5-7 STATION TOTAL PRESSURE RAKE, COBRA PROBES
ORIENTED 120 DEGREES APART, ALIGNED WITH STATIC PRESSURE TAPS

EXHAUST COLLECTOR STATIC PRESSURES
12 PLACES, INTAKE AND EXHAUST PLANES OF
6 PASSAGES IN THE EXHAUST DUCT TO
VOLUTE TRANSITION PLATE.

EXHAUST COLLECTOR ENTRANCE TEMPERATURE
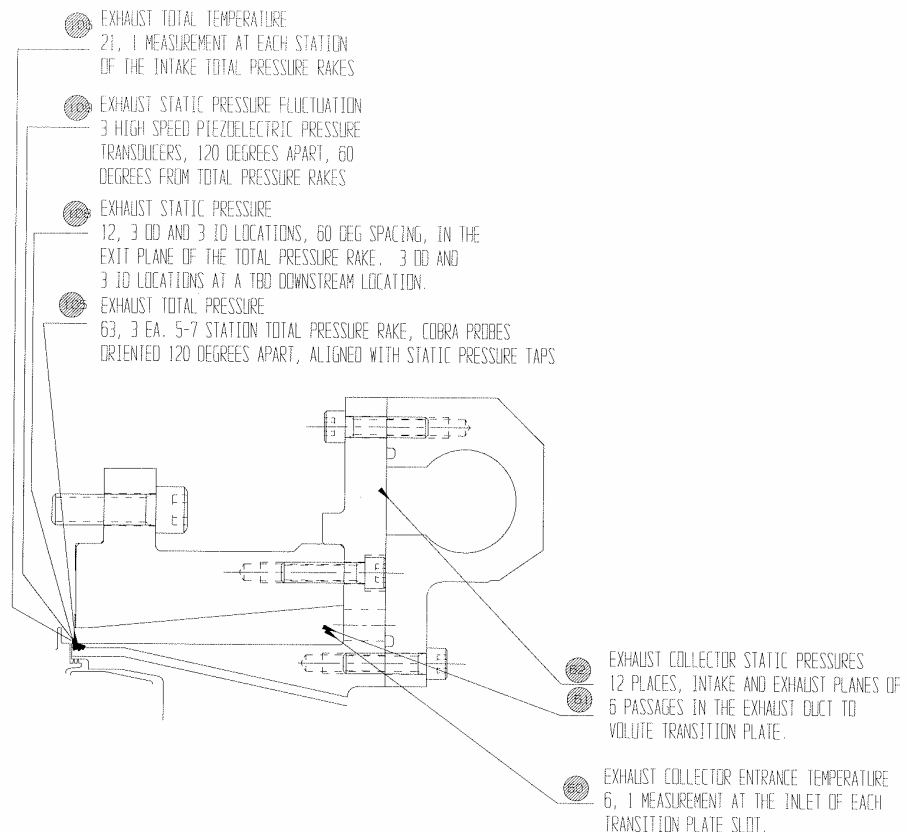6, 1 MEASUREMENT AT THE INLET OF EACH
TRANSITION PLATE SLOT.

Figure 4-39   Example Instrumentation Layout Drawing

BSi RADIAL INFLOW TURBINE DESIGNED FOR 280 PSIG / 400F AIR
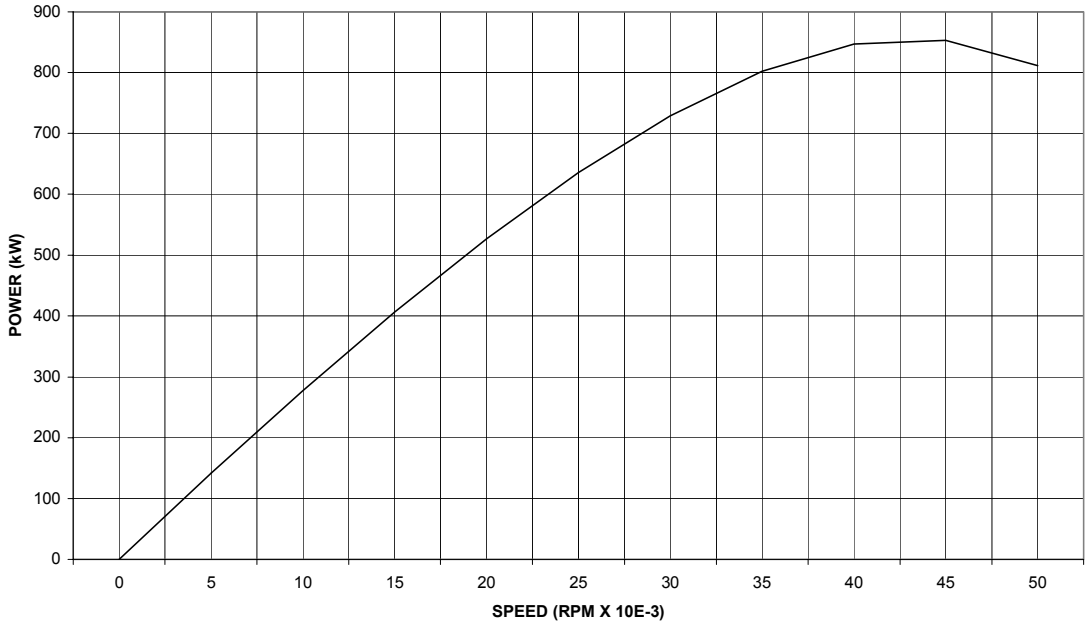**13 LBm/SEC. AT 315 PSIG / 220F**

Figure 4-40   BSi Drive Turbine Power vs. Speed Capabilities.

Condition	Label	AR = 2.2/40506.7 rpm	AR = 1.5/49036.8 rpm
		hp	hp
3	Started with max back P	916	922
4	Un-started with max back P	881.5	908.6

Table 4-3   **Estimates of Rampressor Drive Power Requirements**

Attachment 3-1

Meeting Report

Ramgen Design Review Workshop

April 9-10, 2002